Spring 2021

Vascular Endothelial Dysfunction and Effects on Arterial Wall Microstructure

Jeffrey Thomas Rodgers

Vascular Endothelial Dysfunction and Effects on Arterial Wall Microstructure

By

Jeffrey Thomas Rodgers

Bachelor of Science
University of South Carolina, 2019

Submitted in Partial Fulfillment of the Requirements

For the Degree of Master of Science in

Biomedical Engineering

College of Engineering and Computing

University of South Carolina

2021

Accepted by:

Tarek M. Shazly, Director of Thesis

John F. Eberth, Reader

Susan M. Lessner, Reader

Tracey L. Weldon, Interim Vice Provost and Dean of the Graduate School

Acknowledgments

First, I would like to acknowledge the contributions of my graduate advisor, Dr. Tarek Shazly, in his guidance and mentorship which allowed me to become a more competent researcher, writer, and professional in the field. I would also like to thank Dr. John Eberth and Dr. Susan Lessner, for their contributions and collaboration in providing advice and mentorship in both the project itself and in the further development of my abilities as a scientific and engineering researcher. I would also like to thank Dr. Mohamad Azhar and Dr. Michael Matthews for providing feedback in the drafting and publication of this document. I would also like to acknowledge the contributions of the other former and current students who contributed in some capacity to the completion of this project, namely William Torres, Ph.D., Dara Azar, Ph.D., Brooks Lane, Ph.D., Colton Kostelnik, B.S. for his aid in creating Figure 1.1, Matthew Lohr, and especially Liya Du, M.S., without whom the current progress on this thesis project would not be possible and who greatly aided in collecting the samples used for data in this document. Lastly, I would like to thank my parents, Christopher and Roseanne, and my brother, Craig, for supporting me and being there for me throughout this entire process.

Abstract

Vascular endothelial cell dysfunction (ECD) is a disease characterized by the inability of the vascular endothelial cells to transmit signaling molecules, namely nitric oxide (NO), in response to changes in blood flow rate. This disease is shown to be incident in the onset of more severe vascular disease such as hypertension, atherosclerosis, and heart failure. Long-term ECD is shown to cause long-term remodeling such as decreased flow-mediated dilation, increased pulse-wave velocity, intimal-medial thickening, and increased wall stiffness due to collagen deposition. We used second harmonic generation (SHG) microscopy to analyze this change in the collagen microstructure of the arterial extracellular matrix due to decreased nitric oxide signaling. In the analysis of these microscopic images, we observed a significant increase in the relative frequency of circumferentially oriented collagen fibers with age in knockout mice with an expected decrease in NO signaling compared to their wild-type counterparts. Within these mouse arteries, we also observed a sharper decrease in the tortuosity of the circumferential fibers compared to the axial fibers. Overall, these results have implications toward studies in NO-dependent stress-mediated remodeling and future computational modeling efforts of ECD.

Table of Contents

List of Tables

List of Figures

Chapter 1

Introduction to Endothelial Cell Dysfunction

1.1 Introduction

The structure of elastic arteries consists of three layers: the tunica intima, tunica media, and tunica adventitia (**Figure 1.1**) [86]. The structural proteins elastin and collagen (primarily type I) are the key passive load-bearing components in the arterial wall, while smooth muscle cells are responsible for active force generation. Other wall constituents, notably proteoglycans, play a role in vascular tissue mechanical behavior but are excluded from most continuum-level mechanical models due to the deterministic influences of elastin and collagen [5,67]. The numerous layers of elastin in the elastic arteries give rise to an elastic recoil and functionally dampens nominally pulsatile blood flow, a feature central to arterial homeostasis [47,76].

Collagen maintains arterial structure through a cohesive extracellular matrix (ECM), and notably increases and reorganizes during most instances of vascular tissue remodeling [48,86,104]. While elastin is primarily contained within a membranous structure in the elastic arteries, collagen fibers form a complex multi-directional matrix [86]. Given that taut collagen is a stiffer material in comparison to elastin, growth and remodeling processes that lead to a net increase in collagen mass fraction generally coincide with an overall increase in vascular tissue stiffness, as is commonly seen in pressure-induced remodeling in patients with

sustained hypertension [20,66]. Smooth muscle cells (SMCs) are predominantly circumferentially oriented and mediate vasoconstriction/vasodilation in response to both internal and external stimuli [86]. Maintenance of normal vascular SMC tone as well as transient modulations are facilitated by the vascular endothelium, largely through the release of acetylcholine [66].

The vascular endothelium facilitates the growth and maintenance of the blood vessels. In addition to angiogenesis, which is beyond the scope of this paper, vascular endothelial cells (ECs) are involved in the maintenance of vascular tone through mechanotransduction [66,110]. In healthy tissue, ECs convert wall shear stress into a chemical signal through the stimulation of their glycocalyx layer [86]. This stimulation results in the conversion of L-arginine to nitric oxide (NO), an important mediator in the regulation of vascular tone, by endothelial nitric oxide synthases (eNOS) (**Figure 1.2**) [26,104]. Disruptions in NO signaling and dysfunction of the endothelium can result in the onset of vascular disease- their pathological processes generally termed endothelial cell dysfunction (ECD).

1.2 Background

1.2.1 Endothelial Dysfunction

Endothelial cell dysfunction (ECD) is characterized by an inability of the intimal ECs to translate mechanical stimuli into chemical signals, namely NO, which results in a decrease in NO bioavailability. These disruptions in NO signaling often result in a decreased physiologic potential for endothelium-dependent relaxation/vasodilation [26]. In the healthy endothelium, shear stress caused by

blood flow stimulates the production of NO by eNOS [26,41]. This not only modulates vascular tone and vasodilation but also prevents the accumulation of macrophages and platelets, thereby preventing atherosclerosis [72]. However, various factors can lead to the decreased bioavailability, and therefore decreased activity, of NO.

1.2.2 ROS and Associated Biomolecules

The main factor that determines the bioavailability of NO is the relative concentration of reactive oxygen species (ROS), including superoxide molecules, which bind with NO to produce peroxynitrite and inhibit its activity [41,72,110]. There are many underlying conditions that can cause an increased concentration of ROS in the blood. Elevated localized ROS concentrations are largely due to overactivity of smooth muscle NADPH oxidase, which produces superoxide as a byproduct of its processes [72]. NADPH oxidase activation is linked to increased levels of angiotensin II and thrombin, and is mechanically associated with abnormal cyclic strain due to hypertension [13]. In many instances, low shear stress can also lead to a greater concentration of ROS, being partially responsible for the increased plaque development associated with atherosclerosis [105]. However, abnormally large increases in shear stress can also lead to the increased production of ROS, as is seen in superoxide production that occurs as a result of coronary artery reperfusion during treatment of myocardial infarction [35]. Another common molecular origin is vascular endothelial progenitor cell senescence, where natural aging decreases the renewal of the endothelial layer, causing a lessened ability to produce NO [40].

1.2.3 eNOS Inhibition

ECD can also arise due to inhibition of the eNOS protein and desensitization of the vascular SMCs to NO signaling. ROS directly impacts NO concentrations via direct binding to form peroxynitrite and can also bind with and deactivate eNOS [72]. While this process is seen gradually in aging individuals, eNOS uncoupling and inactivation is replicated in the laboratory pharmaceutically by exposing specimens to L-NAME (N(gamma)-nitro-L-arginine methyl ester) or L-NMMA (L-N(gamma)-monomethyl arginine acetate) [75,129]. The gradual uncoupling of eNOS coincides with aging, but there is evidence to suggest that the pharmaceutical addition of tetrahydrobiopterin (BH_4), an important cofactor of eNOS, can protect against this process and mediate healthy signaling [103,129]. After NO is transmitted to the vascular SMCs, the ability to elicit a response also depends on the local activity of guanylyl cyclase in the production of cGMP (cyclic guanine monophosphate) [71] (**Figure 1.3**).

1.3 Clinical Correlations

1.3.1 Systemic Conditions Can Exacerbate Endothelial Dysfunction

ECD is both the result and advent of numerous systemic conditions (**Figure 1.4**). Previous clinical studies have shown that external and systemic factors such as regular smoking, diabetes mellitus, and a sedentary lifestyle can lead to the onset of ECD. For example, chronic exposure to tobacco smoke leads to decreased NO bioavailability as well as the initial development of hypertension and atherosclerosis [69,80,100]. Specifically, the decrease in NO is correlated with the

transmission of inflammatory, atherogenic signals [69]. Diabetes has been shown to correlate with a decrease in NO bioavailability related to ECD [4,41,104]. One of the likely reasons for this is that insulin facilitates vascular NO production [41,124]. Because regular exercise provides periods of increased shear stress, mechanical stimulation, and decreased oxidative stress, a sedentary lifestyle is also an indicator for the likely onset of ECD [41,62].

1.3.2 Hypertension and Endothelial Dysfunction

Clinical correlations have been observed between hypertension and ECD, with evidence to support that ECD can both cause and be a result of hypertension. In many cases, chronic ECD tends to exacerbate hypertension [3,104], and it is believed that this systemic increase in blood pressure is a result of the lack of microvascular dilation due to NO signaling [20,78]. Likewise, there is a growing body of evidence that agents commonly prescribed to treat hypertension, including calcium channel agonists and angiotensin-converting enzyme (ACE) inhibitors can alleviate the effects of ECD [31,91]. However, other studies debate the correlation between ECD and hypertension, and instead indicate that sustained hypertension appears to cause ECD [85]. These proponents argue that sustained clinical hypertension results in an increased circumferential stretch, causing maladaptive vascular remodeling [115]. This may also be a result of the increased oxidative stress due to the overactivity of enzymes like NADPH oxidase as is seen in some patients with clinical hypertension [91].

1.3.3 Relationship with Atherosclerosis and Vascular Disease

Other studies indicate that ECD may lead to the development of more severe cardiovascular conditions such as atherosclerosis and heart failure. NO, which is maintained by consistent laminar flow of blood within the arteries, is commonly seen as a major atheroprotective factor during normal functioning [18,21,33]. A dysfunctional vascular endothelium is commonly associated with a maladaptive interaction with low-density lipoprotein (LDL) cholesterol in the blood, and there is a direct correlation between hypercholesterolemia and localized ECD [96]. It has also been observed that a deficiency in NO signaling can lead to the initiation of an inflammatory cascade, which can cause platelet adhesion, lymphocyte migration, and eventually atherosclerotic plaque development [72]. Areas that have irregular flow patterns, such as bifurcations, are especially prone to this process [18]. Further progression of atherosclerosis and hypertension through chronic endothelial dysfunction can eventually lead to more severe outcomes such as stroke, myocardial infarction, and heart failure [66]. There is a confirmed link between ECD and the pathogenesis of aortic and cerebral aneurysms through increased oxidative stress, decreased eNOS activity, and activation of the inflammatory cascade [94,95].

1.3.4 COVID-19 and Regionalized Endothelial Dysfunction

Recently, clinical studies have observed a correlation between symptomatic cases of coronavirus disease 2019 (COVID-19) and the onset of ECD, specifically within the cardiac and pulmonary regions. Severe acute respiratory syndrome (SARS) infections, both of previous SARS cases and now of its variant SARS

coronavirus 2 (SARS-CoV-2), cause irregular activation of the inflammatory pathways [30,97]. One such example is in the interference of SARS-CoV-2 in the homeostatic maintenance of the renin-angiotensin-aldosterone system [2,97]. Continuous activation of inflammatory pathways by this virus and increased coagulability, especially within the pulmonary vascular system, can lead to ECD as well as other vascular events such as deep vein thrombosis, ischemia, and stroke [30]. There is also evidence that points to SARS-CoV-2 being able to directly infect vascular ECs, resulting in localized ECD [74]. However, it appears that those patients who have had preexisting ECD being diagnosed with COVID-19 are more prone to adverse vascular events while infected [74]. Thus, lifestyle measures such as diet and regular exercise are key in preventing vascular complications due to COVID-19 within individuals who are part of a more vulnerable population [74]. Overall, because SARS-CoV-2 has deleterious effects on the vascular endothelium, and understanding of the remodeling caused by endothelial dysfunction can provide insight into the management of COVID-19 [64].

1.4 Tables and Figures

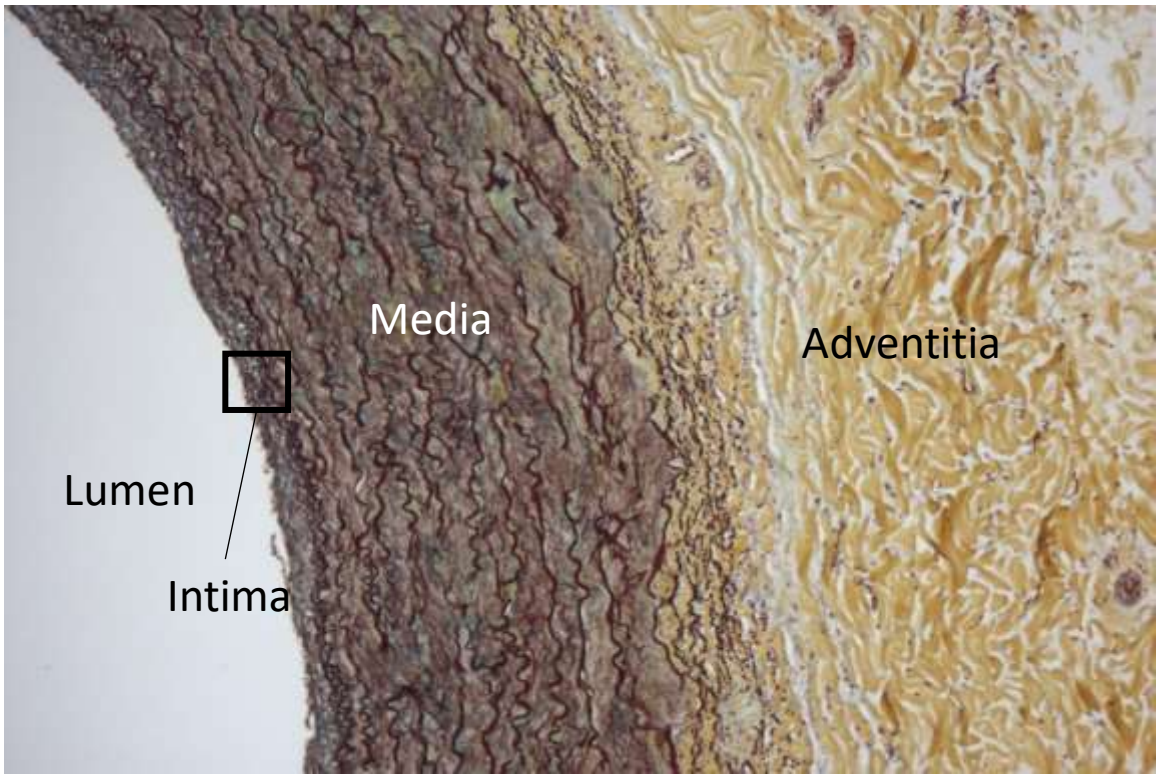

Figure 1.1. Histological cross-section of a porcine internal thoracic artery using Movat's Pentachrome. This figure details the three main layers of the arterial wall which are differentiated by the color oof the stain in the image. As can be seen here, the internal elastic lamina separates the intima from the media, and the media contains multiple elastic layers with collagen scattered throughout. The adventitia is stained differently because it contains mostly connective tissue, including fibroblasts and adipocytes. (Image courtesy of Colton Kostelnik, see also Kostelnik et al., 2021) [58].

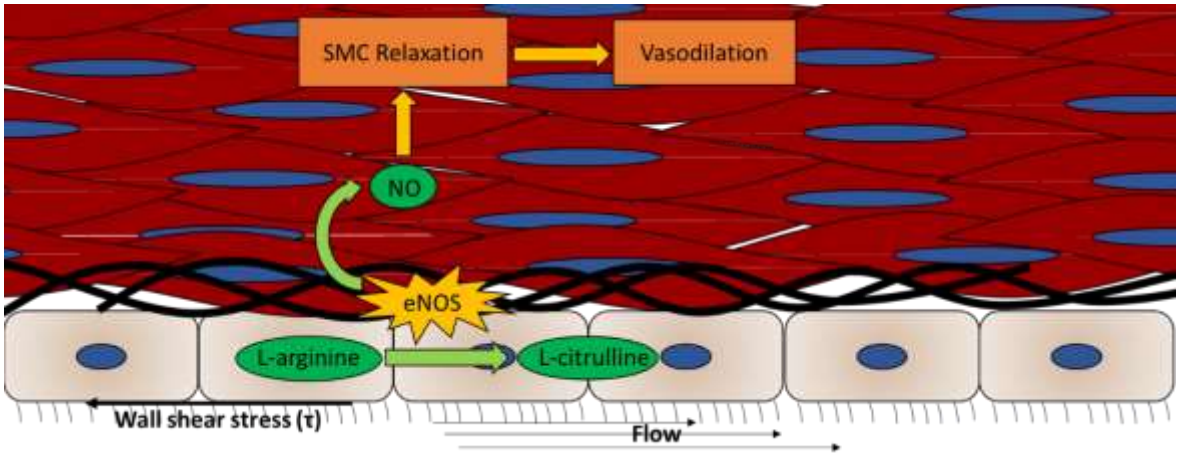

Figure 1.2. Production and effects of NO in a healthy vascular wall. In this diagram, eNOS uses L-arginine to produce NO, which goes on to relax the smooth muscle and dilate the artery. Green arrows refer to products, while yellow arrows refer to effects.

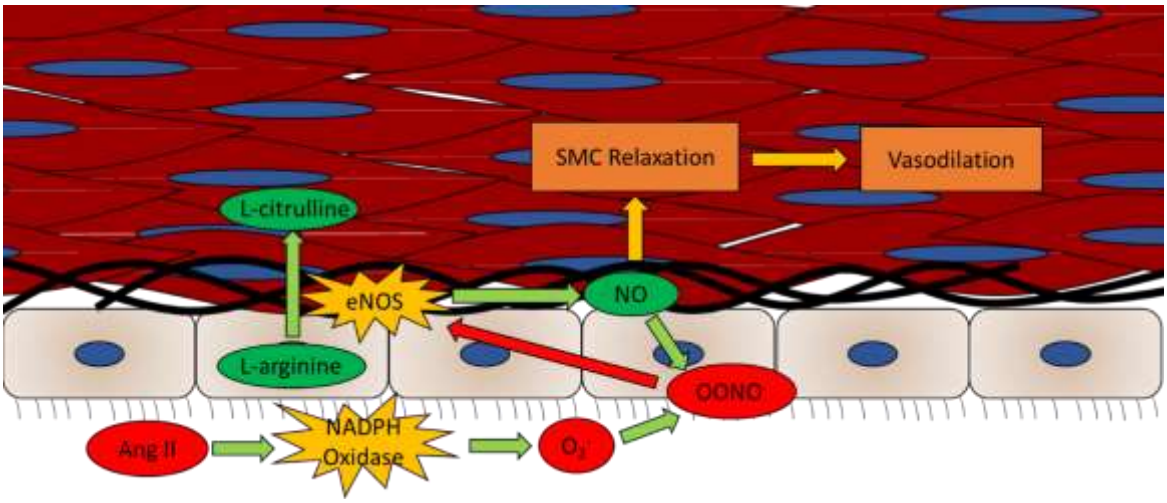

Figure 1.3. Inhibition of eNOS by ROS. The increased presence of angiotensin II (Ang II) stimulates NADPH oxidase, which produces superoxide. This combines with NO to create peroxynitrite, which can inhibit eNOS, preventing proper NO signaling. Green arrows show products and stimulation, yellow arrows show effects, and red arrows show inhibition.

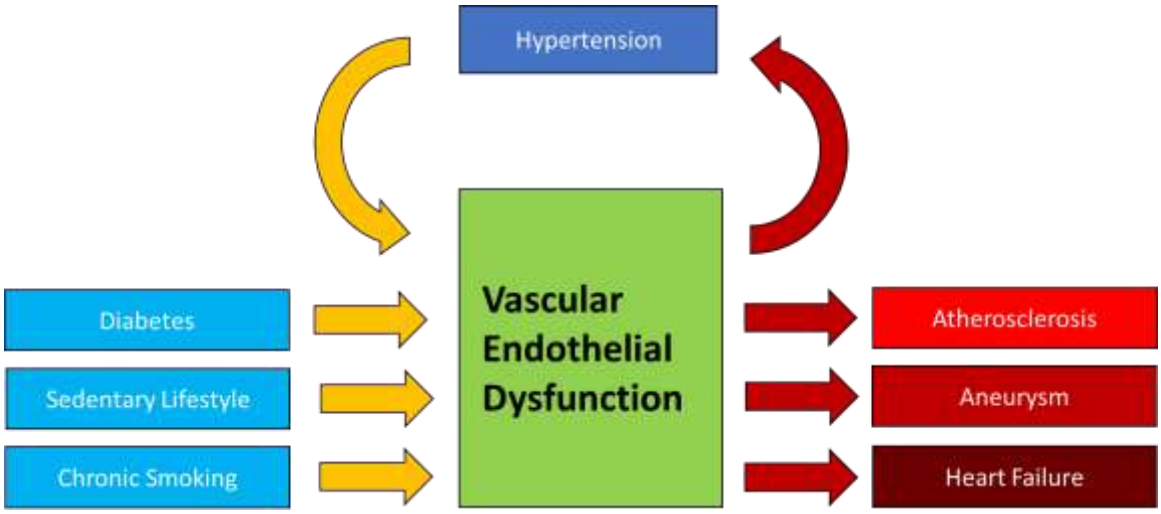

Figure 1.4. Clinical context of vascular endothelial dysfunction/ECD. Systemic conditions associated with the exacerbation of vascular endothelial dysfunction/ECD (blue) are shown on the left, and the vascular diseases affiliated with ECD (red) are shown on the right. As shown above, systemic hypertension is both a contributor to and a result of ECD.

Chapter 2

Review of Experimental Studies

2.1 Flow-Mediated Dilation

Various techniques have been previously used to quantify endothelial dysfunction and its associated remodeling of the vascular wall, including flow-mediated dilation (FMD). In short, FMD uses reactive hyperemia, commonly in the brachial artery, to measure an artery's ability to dilate. The relative percent dilation of the brachial artery is used to quantify endothelial-dependent vasodilation [36]. In this case, arteries that have lower endothelial functioning are less able to adapt to a sudden, temporary increase in the rate of blood flow [57]. While the ability of this method of measurement to predict future vascular outcomes is limited, there is conclusive evidence that changes in FMD percentage (%FMD) across multiple tests can be an indication of developing vascular disease [90].

Previous studies have reported that a decrease in dilation in response to reactive hyperemia corresponds with a decreased endothelial function and serves as an overall predictor of cardiovascular events [36,57,79]. Gocke et al. showed that individuals with noninvasively determined endothelial dysfunction had an average %FMD that was 37% less than that of healthy individuals [33]. This finding is reinforced by Poggianti et al. where in those with more severe vascular diseases, the %FMD can be less than half of that in healthy subjects [79]. Furthermore, there tends to be an inverse relationship between the %FMD and the severity of the

disease with a 17% decrease in cardiovascular risk associated with every 1% increase in %FMD [36,109]. However, Green et al. (2011) have shown that longitudinal decreases in %FMD have the greatest correlation with deterioration in endothelial functioning [36]. Because these longitudinal changes can be minute, this data should be supplemented with other methods of testing to fully assess endothelial functioning [90].

Other studies have also directly quantified eNOS activity through localized NO concentrations or through measurement of the arterial response to stimuli associated with NO activity. Hansen et al. which linked HIV to vascular endothelial dysfunction, measured dilation in response to acetylcholine and revealed a 22% lower relaxation in HIV transgenic versus wild-type specimens [37]. Similarly, Huang, et al. revealed that eNOS knockout mice had an acetylcholine-dependent vasodilation that is 13.7% lower than that of their WT counterparts [43]. Within aging human subjects, dilation measurements via peak flow rate revealed acetylcholine-dependent dilation to be significantly less in aged individuals whereas SNP-dependent dilation was insignificantly different [99,101]. Another technique that is also being used to measure endothelial function is flow-mediated contraction in response to reduced flow [34]. While flow-mediated constriction has not been as extensively studied as FMD, current research suggests that this test, when coupled with FMD, can provide a more accurate assessment of endothelial function [38].

2.2 Pulse-Wave Velocity

Pulse-wave velocity (PWV) is a common technique used to assess the mechanical properties of an artery in-vivo and is mostly used in clinical studies and

in situations where ex-vivo mechanical testing is not feasible [3]. Briefly, PWV measures the time it takes for an arterial pulse-wave to travel between two pressure transducers [63]. This velocity measurement, along with arterial diameter measurements taken with ultrasound, are used to determine the compliance and distensibility of the major artery [63]. A greater pulse-wave velocity measurement is often associated with stiffer arteries due to less absorption of kinetic energy by the elastic membranes [17,92]. Abnormal PWV readings are often associated with diseases such as hypertension [17]. During these types of tests, the ultrasound measurements are often also used to obtain information regarding the compliance and distensibility through incremental measurements of pressure and cross-sectional area, which can be used to obtain the volume of blood contained within the vessel [11].

Within younger adults, a higher PWV can often indicate the onset of ECD, as was determined by relative biomarker concentrations by Van Bussell, et al. and can likely be used as a predictive measure for future vascular disease [14]. When looking at diseases linked with ECD, there is a significant correlation between the level of fasting glucose and mean arterial pressure and PWV [102]. In a more controlled setting with eNOS knockout mice, Jung et al. found that PWV tended to be more than 10% greater in the knockouts compared to the wild-types, along with a similar increase in mean arterial pressure with similar heart rates [49]. An increase in PWV also corresponds to an increase in vascular disease severity (such as atherosclerosis, hypertension and other associated diseases), with the most severe causing an increase of 41% [109].

An increased PWV corresponds with a decrease in compliance and distensibility [6]. In linking childhood obesity to endothelial dysfunction, Tounian et al. found the unhealthy subjects to have significantly decreased compliance and distensibility compared to the control group [108]. These findings of decreased compliance are also found in adult patients with ECD via acceleration of peak velocity, which tends to be inversely related [99]. This significant decrease in distensibility remains true over more gradual periods, through the level of changes varies depending on the location according to Van Bussell, et al. [15]. While some may argue that the above changes observed in these patients are a result of comorbidities rather than ECD itself, these trends were also observed in more controlled experiments with eNOS knockout mice [49,61]. The results from the above two sections are summarized in **Table 2.1**.

2.3 Wall Stiffness

A likely contributor to decrease in compliance and distensibility is an increase in tissue stiffness. Within aging individuals affected by various cardiovascular conditions, those with ECD were reported to have a greater elasticity index compared to healthier controls, which is a numerical factor used as a surrogate for tissue stiffness [101]. This finding is mirrored by studies which have observed a similar phenomenon in children with diagnosed vasoactive dysfunction [15]. However, increased tissue stiffness was not seen in experiments where ECD was induced in transgenic mice and their arterial tissue properties were assessed via ex-vivo biaxial mechanical testing [7,37].

In other studies that examine the trends in stiffness in pathologies correlated with ECD, there is a distinct trend toward increased stiffness. During the biaxial mechanical testing of diabetic arteries with measured vasoactive dysfunction, there is a notable trend toward increased stiffness with age in the circumferential direction compared to healthy controls [23,106]. This corresponds with a doubling of the elastic modulus in arteries affected by ECD along with a decrease in material parameters used to quantify the contribution of collagen to the overall strain energy equation [23]. These overall changes in stiffness due to ECD are mostly reflective of changes in the constituent mass fractions within the medial extracellular matrix, as is seen in studies directly looking at ECD and those looking at correlated disease states such as hypertension [25,108].

While other studies have used biaxial testing to assess arterial mechanical properties, some in-vivo studies have been able to examine these properties through indirect measures such as the augmentation index (AIx). As with FMD and PWV, AIx can be used as a predictive measure for cardiovascular risk [77]. The AIx measures an elastic or peripheral artery's response to a pulsatile pressure, with a greater AIx corresponding with a stiffer artery [3,63]. Like with arterial stiffness, modulation of NO tends to increase augmentation index and causes the arteries to become stiffer [3]. This increase in AIx is also seen in diseases related to ECD [77,121]. Tudoran, et al. shows that the percent increase in AIx is correlated with disease severity [109]. This is further developed in a study by McEniery, et al. which showed that Aix is significantly negatively correlated with endothelial functioning and is directly related with PWV and arterial stiffness [68].

2.4 Intimal-Medial Thickness

Observed changes in wall stiffness and measurements obtained by FMD and PWV due to ECD are accompanied by alterations in arterial geometry and relative amounts of constituents within the arterial wall. As is observed in eNOS knockout mice, one of the key characteristics that arise as a result is increased intimal-medial thickness (IMT) [41,72,85,88,123]. While studies such as Poredos, et al. that looked at ECD in terms of other conditions quantified the increase in IMT at around 10%, Kleinbongard et al. isolated this disease and observed changes of up to 60% [55,80,123]. Not surprisingly according to Yuskel, et al. increased IMT is coupled with an increase in the arterial cross-sectional area [130]. While smooth muscle hyperplasia is also observed in many cases, increased deposition of extracellular matrix material provides a significant contribution to this increased thickness [37,88]. Most of this ECM expansion is due to an overproduction of collagen, a much stiffer material than elastin [27,37].

Coupled with this collagen expansion is often the gradual degradation of elastin [117]. In ECD, an inversion of the collagen-to-elastin ratio from mostly elastin to mostly collagen is often observed (from ~0.5 to ~2.0) [7,81]. As is shown in Tong, et al., this trend is also seen in diseases correlated with ECD [106]. This conversion of the tissue in the arterial wall from elastic to collagenous explains the increase in the elastic modulus reported by some studies [7,44]. Most of these changes are very much like those observed in the early stages of hypertension [19,91]. Thus, when considering a potential arterial growth and remodeling mechanism, that of hypertension likely provides an excellent framework that can be adjusted to

account for the nuances of vascular ECD [70]. Most of the above information regarding stiffness and IMT is summarized in **Table 2.2**.

2.5. Tables and Figures

Table 2.1. Summary of Experimental Flow-Related Measurement Values

Study	Condition Group	Δ %FMD (%)	Δ PWV (%)	Δ Compliance (%)	Δ Distensibility (%)
Tounian, 2001	Obesity	-44.44	N/A	-7.69	-16.67
Gocke, 2003	Peripheral Vascular Disease	-37.14	N/A	N/A	N/A
Poggianti, 2003	Aortic Valve Sclerosis	-58.49	N/A	N/A	N/A
Tao, 2004	Aging	-10.5	N/A	N/A	N/A
Tedesco, 2004	Diabetes and Hypertension	N/A	46.8	N/A	N/A
Van Bussell, 2011	Aging	N/A	7.79	-23.53	-20.55
Tudoran, 2015	Hypothyroidism	-78.40	40.81	N/A	N/A

Summary of experimental values pertaining to previous studies which examined the flow-related properties of arteries with vasoactive dysfunction *in-vivo*. To the left is the name of the study, followed by the condition group measured by the study, and the percent difference in parameters of the affected group compared to the control group. The results of these studies are summarized at the bottom row using averages. All studies are conducted with human. Studies marked with an asterisk (*) indicate those in which dilation was achieved using acetylcholine as opposed to using FMD. All quantities represented are associated with a p-value of $p<0.01$ [15,33,37,43,79,101,102,108,109].

Table 2.2. Summary of Experimental Structure-Related Measurement Values

Study	Condition Group	Δ E (%)	Δ AIx (%)	Δ IMT (%)
Poredos, 1999	Smoking	N/A	N/A	15.25
Wilkinson, 2000	Diabetes	N/A	>90	N/A
Tounian, 2001	Obesity	75	N/A	N/A
Woo, 2004	Obesity	N/A	N/A	8.89
Kleinbongard, 2006	Elevated plasma nitrite levels	N/A	N/A	60
Eberth, 2011	Hypertension	N/A	N/A	75.32
Van Bussell, 2011	Aging	4.55	N/A	6.45
Tudoran, 2015	Hypothyroidism	N/A	23.77	45.16
Yuksel, 2016	Bechet's disease	N/A	N/A	25.42
Desyatova, 2017*	Aging and Diabetes	N/A	N/A	37.22

Summary of experimental values pertaining to studies which examine the structure-related properties of arteries affected by ECD. The left column represents the name of the study, followed by the condition group studied and the measured quantities. The values are summarized by averages given at the bottom row. All studies are conducted with human subjects or samples. All IMT measurements were taken at the carotid arteries. Studies marked with an asterisk (*) denote those here the total wall thickness is reported instead of IMT. All quantities represented are associated with p-values of $p<0.05$ [15,23,25,55,80,108,109,121,123,130].

Chapter 3

Review of Mechanical Modeling

3.1 Introduction

To accurately model ECD, one must choose a modeling framework from which to operate. Previously, arterial mechanical behavior has been characterized through several different approaches. Many studies have used phenomenological models to represent this mechanical behavior, in which experimental results are used to populate the strain energy equations. While this method of characterization is highly useful in being able to accurately assume a mechanical model from experimental data, it lacks many of the predictive capabilities that other modeling methods provide [47,116]. A second classification of mechanical behavior is a structurally motivated model, in which the mechanical behavior is characterized by a combination of the individual constituents of the artery via a mixture model [60,83]. This type of model more adequately describes the mechanical behavior of the arteries through the inclusion of collagen, elastin, and smooth muscle contributions [12,113]. As will be discussed, many previous studies have expanded upon this notion by categorizing constituents by their respective layers through multi-layer models throughout the different stress states shown in **Figure 3.1** [113]. To better study the changes surrounding the growth and remodeling associated with a disease state, some studies add growth and remodeling kinetics that consider the changes in

constituent geometries and relative contributions to the strain energy equation over time, as shown in **Figure 3.2**. Other studies have expanded upon this by also accounting for interactions between the constituents at the cellular level through chemo-mechanical models [53,54]. However, most agent-based or chemo-mechanical components of these models are beyond the scope of this paper due to their conflicts with the basic length-scale assumptions of continuum mechanics [47,54]. Refer to **Appendix A** for the development of the appropriate kinematic definitions for these models, **Appendix B** for the development of their constitutive equations, and **Appendix C** for the implementation of a G&R approach.

ECD can be defined as an increase in flow rate without compensatory vasodilation [45]. Thus, a modification of maladaptive growth and remodeling due to increased blood flow may also prove useful in the creation of a mechanical simulation. While most of these studies simulate the initial vasodilation due to a modification of active stress, most of the changes in properties associated with the structure of the arterial wall are observed over longer time periods. However, very few studies have explored these changes. Therefore, more work must be accomplished within this condition to gain a further understanding of the mechanical conditions to which ECD corresponds. In an experimental setting, many studies use tests like biaxial mechanical testing on a harvested tissue or flow-mediated dilation on a tissue *in-vivo* [127]. However, there are many times when the simulation of a diseased state is more approachable in terms of time and cost. The following section of this paper is dedicated to the presentation of simulated results from the previously mentioned mechanical models.

3.2 Prediction of Effects of ECD using Related Disease States

The computational mechanical models presented below look at the potential to model ECD like that of associated disease states through previously established G&R relationships. While these studies provide a basis from which an applicable constituent-dependent G&R relationship may be derived, they must be refined to account for the nuances of ECD such as NO-mediated G&R relationships.

The model used by Wan et al. (2010) simulates the changes in arterial structure under a more generalized growth and remodeling framework. After a test in which the remodeling rates of each of the constituents were the same, these authors assumed insignificant elastin remodeling and very similar collagen and smooth muscle remodeling rates. For increased flow rate, the vessel never completely restored its initial circumferential stress. Another finding is a significantly increased collagen deposition in the tunica media under these conditions. For their increased pressure simulations, after inducing maximal smooth muscle contraction the arterial wall increased to twice its original thickness while never completely restoring the normotensive circumferential stress. While this model provides great utility for generalized G&R considering that it accounts for the distribution of newly formed collagen fibers, it lacks the increased complexity of the collagen fiber arrangements that the newer models improve upon [119].

Valentin et al. (2011) applies a G&R strategy to aging. This simulation confirms the clinically observed finding that arteries tend to become less elastic

with age because of gradual elastin degradation and increased collagen deposition. This is seen as an inversion of the collagen-elastin ratio that is observed in the healthier years of adulthood, with the rate varying based on the G&R rate parameters. A gradual decrease in the opening angle with age after thirty years old was also observed, along with an irreversible increase in both vessel wall thickness and mean circumferential stress. For modeling endothelial dysfunction, this model could serve as a good start for building a framework. Some of the key hallmarks of this model are the definition of equations for stiffening of the vessel wall and progressive vasoactive dysfunction. However, this model makes some large assumptions to simplify the equations with respect to collagen fiber deposition and changes in the different layers of the arterial wall [113].

Karsaj and Humphrey (2012) attempt to use a slightly modified approach to G&R, accounting for differences within the different layers of the artery. This was largely done through approximations of both the distance of each layer from the lumen and the mass fractions of each constituent in each layer. Under a simulation of increased pressure, the outer radius was significantly increased, and a significant amount of growth was observed in the media and adventitia. Under increased blood flow, only a slight increase in inner and outer radius was observed and there was no evidence of remodeling. Under hypertension and conditions more representative of a diseased state, a significant increase in the outer radius was observed along with a decrease in the opening angle. This study improves on previous models of G&R through the introduction of a multilayered approach, accounting for the differences in composition among the layers. However, with this

added level of complexity it also simplifies the collagen structure by not accounting for fiber angle or change in collagen structure during deposition. During its simulation of G&R in the diseased state, it also made assumptions in its parameters based on clinical findings rather than establishing predictive equations as was done in the previous studies [51].

The model introduced by Valentin, et al. (2013) expands upon a constrained mixture approach with the use of differential G&R for each of the constituents. Finite element analysis then simulates the stress and strain under differential growth. During their simulations, these authors discovered a modest decrease in circumferential stress, a modest increase in axial stress, and arterial loss of mass during homogeneous growth and remodeling. For G&R applied differentially to the constituents, production of both circumferential and helical collagen fibers as well as growth rate for smooth muscle and adventitial collagen increased significantly over time. However, this same trend was not observed in terms of the applied stresses. The key advantage to this model is the application of the constrained mixture theory for both finite element and semi-analytic approaches, demonstrating the true practicality of this simulative environment. By using an integral rather than a differential approach, the history of the vessel can be considered. However, this model is more for general G&R rather than application to a specific diseased state, so applying it to ECD or another diseased state requires an intermediate analysis into the true observed remodeling rates of the constituents under these diseased conditions [114].

Shazly and Rachev (2020) further expand upon the constrained mixture model for growth and remodeling by adding a more thorough definition of collagen fiber angle and adding fiber recruitment into the strain energy equations. The interaction between collagen and elastin is also included within the mixture model, causing a change in the recruitment of collagen fibers. Instead of using equations to account for the continual production and decay of each constituent, this model simply uses a starting and ending point for each constituent's mass fractions during hypertensive G&R based on the change in loading conditions. The key advantage of this model is the increased complexity of the collagen matrix being considered in the definition of the constitutive equations. While the embodiment of G&R in this study pertains strictly to hypertension, the similarities in changes between hypertension and endothelial dysfunction can allow this level of remodeling to be considered. However, the homeostatic pressure-dependent growth and remodeling considered in this paper prevents its easy utility in cases such as ECD [84].

3.3 Predicting Effects of ECD using Change in Pressure

Concerning the computational modeling of ECD, studies often refer to the maladaptive remodeling in response to changes in blood flow. Maladaptive remodeling, in contrast to adaptive remodeling, evolves because of an inability to restore mechanical properties such as shear stress and stress within the wall. This type of remodeling often results in permanent changes in the unloaded arterial geometry. Within the model developed by Rachev (2000), passive and active mechanical properties along with G&R kinetics were defined to predict the

macrostructural changes of elastic arteries. This study characterized these changes due to remodeling as a remodeling stretch ratio, which defines the remodeled arterial geometry as a ratio between the final unloaded length to the initial unloaded length. During shorter time periods, the smooth muscle was able to adequately restore the wall shear stress but had a gradual decay in its vasoactive stress contribution over longer time periods. Over these longer time periods, the study also observed that the degree of increased flow rate is correlated with the total increase in both median radius and wall thickness, much like the previously discussed histological analyses of arteries with ECD. There was also a slight decrease in inner radius over longer time periods. Overall, these changes due to remodeling were able to restore the geometry such that there was no observable remodeling stretch ratio at lower flow rates and a remodeling stretch ratio of less than 1.1 at higher flow rates. Therefore, the remodeling that occurred to restore the initial stress state did not produce a large change in arterial wall geometry [82].

Maladaptive tissue remodeling due to increased flow rate is further defined by Humphrey and Rajogopal (2003), who modeled collagen deposition in response to a step change in blood flow. This study uses homogenized constrained mixture theory in defining the stress functions, along with added components to account for constituent evolution over time. As such, this study describes constitutive equations for each of the three main load-bearing components of the artery. In describing their remodeling rates, these authors assumed that collagen deposition occurs at a preferred stress state with the goal of restoring the wall stress before

the occurrence of abnormal loading. Their assumed remodeling rates account for remodeling due to both contraction and dilation that occurs in response to the endothelial release of signaling molecules. They found that a 30% increase in flow rate was accompanied by a 10% increase in diameter over longer time periods at which maladaptive remodeling occurs. This was largely assumed to be a result of collagen deposition and production of new smooth muscle, much like in arteries experiencing ECD. However, this study was unable to further extrapolate the resultant remodeling from their constitutive equations because of the lack of studies at the time of publication on the material parameters and both the rates of change and the survival fractions of the constituents [46].

Gleason and Humphrey (2005) expand upon this previous work through a constrained mixture model with differential constituent growth kinetics and a more detailed definition of the collagen matrix. As in the previous models, the rates of mass production and turnover are directly influenced by the difference between the current and homeostatic wall stresses. In accounting for collagen, however, these authors used a two-term Gaussian distribution to define the angular distribution of the fibers in the collagen matrix. They also defined the smooth muscle contributions such that shear stress was almost instantaneously restored by smooth muscle activity, followed by long-term constitutive G&R to restore the homeostatic wall stress. After increasing the rate of flow three-fold, they explored the changes in arterial geometry and constituent mass fractions under both equal and variable constitutive remodeling rates. Under equal remodeling rates, the wall thickness and loaded radius increased by about 40%. When the growth rate was

greater than the turnover rate, a decrease in wall shear stress was coupled with a sharp increase in wall thickness and loaded radius that eventually settled at an overall 40% increase from the initial state. When turnover rate was greater than growth rate, the wall thickness decreased before both loaded radius and wall thickness sharply increased by 40% overall. This is coupled with an initial increase in stress before homeostatic stress was restored. These latter two cases have implications in ECD-related arterial wall remodeling in their assumption of smaller changes in elastin with extensive collagen deposition. While heightened growth rates could simulate changes that can result in systemic hypertension, heightened turnover rates could have implications in ECD-related aneurysm development. In all cases, there was no long-term change in constituent mass fractions. In all remodeling cases, the authors mention that the medial SMC are replaced with ones with a different vasoactive range [32].

Another study by Valentin, et al. (2008) further explored the contribution of smooth muscle activity through the shear stress-mediated modulation of constriction and dilation in a constrained mixture model [111]. To account for collagen deposition, they utilized a mass production rate based on the change in stress of the collagen and smooth muscle [111]. Over longer time periods, they observed that a 30% increase in flow rate caused the inner radius of the artery to increase by almost 90% [111]. This increase in radius allowed for the restoration of a homeostatic wall shear stress [111]. In a sequential study following a similar mechanical setup with collagen being deposited at a certain residual stress, they were able to vary G&R with the level of generated active stress, [112]. Because less smooth muscle

activity results in less active stress, the stiffness parameters of the arteries must often increase to compensate, as is seen in arteries affected by ECD as previously discussed [112]. This lack of SMC active stress generation is a direct representation of the effects of lower NO signaling due to ECD, as discussed previously. As a result, the required increase in stiffness is related to the rate of collagen production [112].

The model used by Wan et al. (2009) simulates the changes in arterial structure under a 3D constrained mixture of constitutive G&R, where the mechanical properties are individually defined. As with many of the previous studies, the kinetic mass deposition rate is a function of the difference between the homeostatic and resultant circumferential stresses. Collagen fibers were assumed to be deposited with a normal angular distribution with a mean located at the preferred direction of stress. The growth rate is also determined by the degree of active stress generated upon the imposition of increased blood flow in the lumen. In a simulation assuming equal constituent remodeling rates and a 60% increased flow rate, the wall thickness increased by 26% over longer remodeling periods. After this test, these authors assumed insignificant elastin remodeling and very similar collagen and smooth muscle remodeling rates. Under these conditions, the thickness increased by 24% and the vessel never completely restored a steady-state circumferential stress. Another finding is significantly increased collagen deposition in the tunica media under these conditions. These physiological remodeling rates involving gradual elastin decay along with SMC proliferation

coupled with collagen deposition is directly related to the findings associated with ECD-related maladaptive remodeling [119].

Wu and Shadden (2015) further extend the above developments by coupling hemodynamics into their growth model to allow for G&R to be observed over a more patient-specific aneurysm geometry under variable pressure. Within this kinetic model of constitutive growth, they developed upon the previous models by introducing differential growth patterns for the load-bearing components of the arterial wall. By assuming that most of the elastin is produced prenatally, it was modeled using a first-order decay function, while collagen used a stress-mediated growth function like those in the previous models and experimental studies related to ECD. In the initial homeostatic stress configuration, most of the stress was borne by collagen fiber families oriented in the 45° and 135° (±45°) directions. Upon the application of shear stress, the loss of mass in the arterial wall close to the bifurcation led to inflation and expansion of the aneurysm. This led to a reduction of stress along the two previously mentioned fiber families. One thing to note, however, is that this study assumes that blood is a Newtonian fluid exhibiting Navier-Stokes behavior. While this assumption may hold for larger arteries with simple geometries, it is not as valid when applied to situations with smaller arteries and more complex geometries [125].

3.4 Summary of Results and Predictions

While more details should be integrated into the above models to properly account for the recent advances in our understanding of ECD, they can be used in future computational studies. Because ECD is often viewed as an increased flow

rate without vasoactive mechanical compensation, the results from most of these models after the period of initial vasodilation may be extrapolated to predict the long-term remodeling in this disease [45]. Overall, the above studies observe an increase in arterial diameter and wall thickness over time to restore the smooth muscle to a homeostatic equilibrium. They also conclude that most of the wall thickening is a result of increased collagen deposition, which increases the stiffness of the vessel [46,112].

While these studies fail to address the nuances associated with vascular endothelial dysfunction, they can still be used as a basis for future modeling of this disease. They may also be improved by addressing the increased complexity of the collagen matrix, even beyond the distribution functions that some studies have presented. One example of such an improvement accounts for not just the direction but also the tortuosity at which collagen is deposited [84]. Another improvement may be to couple flow-mediated remodeling with that which occurs due to aging, a factor that likely needs to be accounted for because of the effects of cell senescence which is often observed in endothelial dysfunction [40,113]. However, more experimental data will likely be needed if model development is to be accurate.

3.5 Tables and Figures

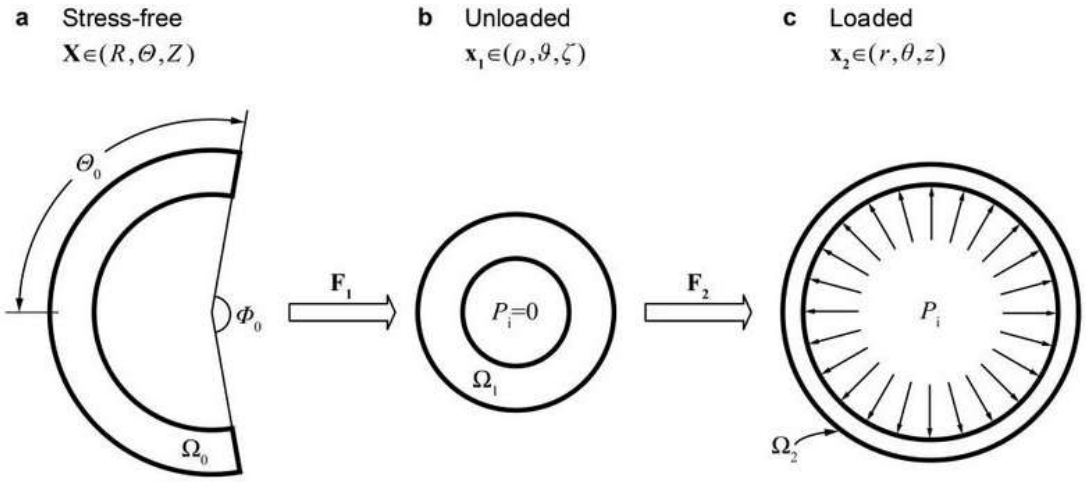

Figure 3.1. (Adapted from Yang, et al.). Depiction of the three primary mechanical states of the arterial wall from which kinematic definitions are determined. **A)** The stress-free configuration, which is obtained by cutting through the thickness of the artery, is fully equilibrated after release of the residual stresses held by the structural collagen and elastin. **B)** The unloaded configuration has no internal stress applied but maintains the natural wall stress acquired from the structural collagen and elastin. **C)** The loaded configuration represents the arterial wall in its natural state, with an applied internal pressure [128].

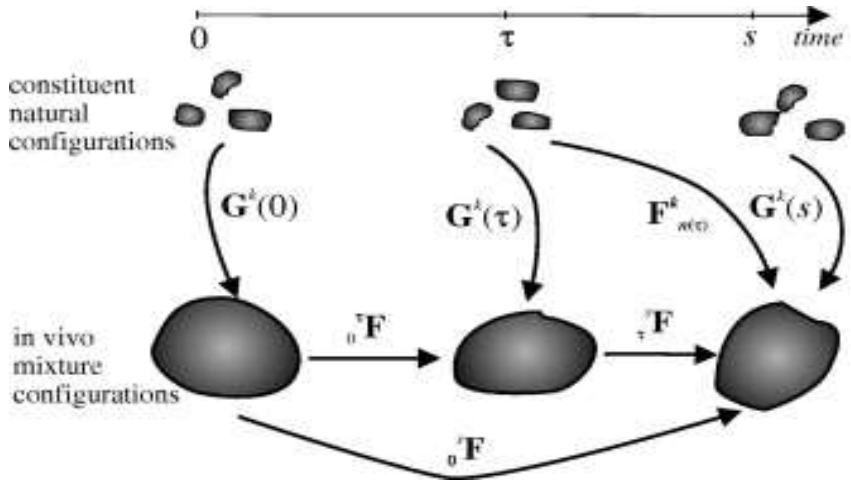

Figure 3.2. (Adapted from Karsaj, et al.) Depiction of the main development states important for defining constituent growth and remodeling. In between the initial time “0” and the final time “s”, there is a gradual permanent deformation of the constituents with the purpose of adapting to the altered mechanical state and restoring the homeostatic wall stress. The natural configurations are stress-free for each constituent. Kinetic deformations in between the initial and final time points are considered to be at a generic time “τ” [52].

Chapter 4

Changes in Vascular Microstructure

4.1 Abstract

Vascular endothelial dysfunction is often viewed as the onset to severe vascular disease. Caused by the lack of nitric oxide signaling by the endothelium to the vascular wall, it often results in the inability of the smooth muscle to dilate in response to changes in blood flow rate. In this study, the aortas of three different groups of mice-- wild-type, eNOS/NOS3 knockout, and heterozygous--- at various ages were stained and imaged using second harmonic generation microscopy. The collagen fibers in these images were then grouped into histograms based on their tortuosity/undulation and their orientation relative to the axial direction. The fiber orientation was classified in terms of four quadrant families: axial, circumferential, and two helical. Since ECD is often characterized by a lack of smooth muscle vasodilation in response to increased blood flow, we predict that the arteries of those mice with decreased endothelial NO signaling will have a greater relative amount of circumferentially oriented collagen fibers because of maladaptive remodeling to increased wall shear stress due to blood flow. In this study, there was an observed increase in the relative frequency of fibers in the circumferential family with age within the knockout mice compared to the wild-type group. Regarding changes in tortuosity, the observed alteration was less drastic

outside of a slight increase in the undulation of the axial fibers in the knockout mice over time. There was also no noticeable difference between the heterozygous groups with partial endothelial NO signaling and the wild-type groups in terms of overall fiber orientation, indicating that loss of a single copy of the NO synthase gene does not produce a significant change in the microstructure of the vascular wall.

4.2 Introduction

With the increasing prevalence of vascular disease, the search for possible treatments has become increasingly relevant. While diseases such as hypertension, atherosclerosis, and heart disease have been extensively studied, there remains a gap in understanding concerning one of the precursors to these diseases, known as vascular endothelial dysfunction or endothelial cell dysfunction (ECD) [3,20,63,72]. Even though endothelial dysfunction is often clinically associated with hypertension, there are also other conditions that can cause it to develop independently of hypertension [10,19,91]. While ECD tends to be a normal consequence of aging as a result of endothelial progenitor cell senescence, it has been shown to be exacerbated by conditions endemic to the Western world such as diabetes, chronic smoking, and a sedentary lifestyle [86,100,124].

At its core, ECD is the inability of the vascular endothelium to adequately regulate vascular tone through the dilation of smooth muscle [129]. In the healthy endothelium, shear stress caused by laminar flow stimulates the production of nitric oxide (NO) by endothelial nitric oxide synthase (eNOS) [26,41]. NO not only modulates vascular tone and vasodilation but also acts in preventing the

accumulation of macrophages and platelets that leads to the development of atherosclerosis, [72]. The decreased bioavailability, and therefore decreased activity, of NO can result in vascular endothelial dysfunction [28]. While ECD starts out as a biomolecular disease, measurable changes in the physiological behavior of arteries may indicate future progression into a more severe disease.

Many of these measurable changes in the mechanical behavior during ECD, such as alterations in FMD and PWV, are a result of changes in wall structure and composition. ECD hinders the vascular wall from undergoing NO-mediated vasodilation [72]. As a result, the arterial wall must compensate to handle changes in blood pressure. One of the key components of ECD is an increase in intimal-medial thickness (IMT) [41,85,88,123]. Most of this increase in IMT is due to an overproduction of collagen, a much stiffer material than elastin [27,37]. Often coupled with collagen overproduction is the gradual degradation of elastin [117]. Consequently in ECD, an inversion of the collagen-to-elastin ratio from mostly elastin to mostly collagen is often observed [7,81]. This overproduction of collagen in the arterial wall likely explains the increase in the elastic modulus [7,44].

While the signaling associated with ECD and general trends in arterial histology have been extensively studied, the specific changes in arterial microstructure and mechanical properties are not well defined. There is a need to investigate how ECD affects the orientation of collagen fibers, as well as how both the changes in collagen organization and composition affect the mechanical behavior of elastic arteries. Therefore, this work investigates the effects of ECD and changes in NO signaling on the composition of the extracellular matrix with

increasing age using an eNOS/NOS3 knockout mouse model. We quantify the corresponding change in wall properties through a characterization of collagen distribution within the lower thoracic aortas of these mice. With this knowledge, arteries under ECD can be more completely characterized in future mechanical models.

4.3 Methods

4.3.1 NOS3 Mouse Model

To appropriately analyze the contributions of nitric oxide signaling to collagen microstructure and composition, nitric oxide synthase (NOS3) knockout (KO), heterozygous hybrid (HET), and wild-type (WT) mice on a C57BL/6J (-B6) background, mice were used as animal models in the study (Jackson Laboratories). The genotype of each mouse was determined using PCR. For these mice, the WT group is expected to experience normal vascular NO signaling, where the only deviations from healthy signaling levels are a result of aging. On the other hand, the KO group lacks the gene that allows endothelial cells to produce effective eNOS enzymes and thus is expected to have minimal levels of NO signaling. The HET group is a hybrid of the KO and WT mice, from which partial NO signaling can be expected. From each group, six mice were euthanized via carbon dioxide asphyxiation at a range of ages from 6 weeks to 12 months with the help of our collaborators. From these mice, aortas were relaxed in-situ by our collaborators in 10^{-5} M sodium nitroprusside (SNP) and fixated in 4% paraformaldehyde via pressurized perfusion-fixation, causing a circumferential stress of up to in-vivo conditions loaded to 100 mmHg (λ_z~1.6, λ_θ~1.4-1.5). From

these arteries, segments between the 5th and 6th intercostal branches were dissected for imaging.

4.3.2 Image Acquisition

To allow for the imaging of elastin, collagen, and cell nuclei, excised sections of the arteries were stained with propidium iodide (1:3000 dilution), opened longitudinally, flattened, and mounted within an imaging spacer sealed with a glass cover slip. Two segments from each artery were imaged by our collaborators under second harmonic generation microscopy (SHG) using a confocal multiphoton microscope (Leica SP8) starting from the adventitia through the depth of the artery, resulting in a z-stack of images for each segment. Collagen was imaged using an excitation wavelength of 880 nm (infrared) and an expected emission wavelength of 440 nm. Elastin was imaged using an excitation wavelength of 488 nm (visible laser) and gathered using a band-pass filter for an expected emission wavelength range of 490-530 nm. The nuclei (most of which are SMCs) were imaged using an excitation wavelength of 552 nm (visible laser) and gathered with an expected emission wavelength ranging between 580-620 nm. The elastin, collagen, and nuclei to be recorded in the red, green, and blue channels, respectively. Images were taken at 1 μm increments through the entire thickness of the sample at the two different sites on the same section of the artery.

4.3.3 Image Processing

Appropriate analysis of the extracellular matrix microstructure requires the quantification of the directionality of each of its components. Thus, the z-stack of

images acquired from the previously conducted multiphoton microscopy was first processed using the fiber tracing program in AMIRA (ThermoFisher) to analyze both the collagen fibers and the smooth muscle cell nuclei [120]. Although most of the stained nuclei were SMCs, not all the nuclei that stained in this channel corresponded to a cell of smooth muscle. Therefore, the majority SMC assumption allowed for the median nucleus direction to be taken as the representative direction for the smooth muscle.

The spreadsheets of points obtained from this fiber tracing were then input into a custom MATLAB program for spatial processing [107]. Using vector analysis within this code, the median orientation of the smooth muscle cell nuclei was measured for each sample, as shown in **Figure 4.1**. Assuming that the median SMC is oriented in the circumferential direction, the angle associated with the axial direction for collagen fiber analysis was computed. The output is a data set containing an orientation angle relative to the axial direction (ranging from 0-180 degrees) within the axial-circumferential plane, an elevation angle relative to the axial-circumferential plane, and the fiber tortuosity.

Prior to regression modeling, the acquired set of data was then filtered to remove any outstanding artifacts and outliers, including observations with an elevation angle greater than 50 degrees and a tortuosity greater than 2. The purpose of limiting elevation angles greater than 50 is because most previous studies observed almost all load-bearing collagen fibers to exist within the axial-circumferential plane [118]. All fibers with a measured tortuosity greater than 2 were

filtered out because it is very unlikely that these fibers will become load-bearing within normal physiological functioning [42,83].

4.3.4 Regression Analysis and Modeling

To achieve an accurate representation of the collagen within the extracellular matrix for quantitative analysis and future modeling, histograms were developed for both the orientation angles and tortuosity of the collagen fibers, a variation on the approach of Wan et al. [118]. For the orientation analysis, bins of 10 degrees were established for the range of 0-180° while bins of 0.025 were established for the tortuosity analysis for the range of 1.0-1.5. This abbreviated range for tortuosity analysis was chosen because this range of collagen fibers is the most likely to contribute to the arterial mechanical properties within the normal physiological loading range. The histogram results for both sites were averaged for each specimen.

For tortuosity/undulation, the generated histograms for a group were averaged to generate a representative distribution curve for each group. Because of the intragroup variability among the primary orientation of the collagen fibers, the histograms containing the mean normalized frequencies for each specimen were used to fit a characteristic distribution curve using the Curve Fitting toolbox in MATLAB. After omitting all non-convergent fitted solutions, the parameters for each orientation angle distribution curve were averaged to create a characteristic distribution curve for each group. For orientation angle, a three-term Gaussian distribution was used to adequately represent the fiber distribution, represented by **Equation 1**. For tortuosity, a two-term Gaussian distribution was determined to be

adequate, where an adequate representation is characterized with $R^2 > 0.90$. These representative curves will facilitate the accurate representation of the collagen fiber matrix in future microstructurally motivated models of the vascular extracellular matrix.

Equation 1. Representation of a three-term Gaussian distribution function, where a_i, b_i, and c_i for i=1,2,3 are constants determined by residual analysis in MATLAB and x is value of the parameter being measured. For the two-term Gaussian distribution function used to represent tortuosity, the same equation is applied but only for i=1,2.

$$f(x) = \sum_{i=1}^{3} a_i * \exp\left(-\left(\frac{x - b_i}{c_i}\right)^2\right)$$

4.3.5 Fiber Family Statistical Analysis

The collagen fibers for each sample were separated into four equally sized quadrants by fiber family classification, with one axially-oriented, one circumferentially-oriented, and two helically-oriented families (axial= 0-22.5°; 157.5-180°, circumferential= 67.5-112.5°; helical= 22.5-67.5° and 112.5-157.5°) using MATLAB. For each family in a sample, the mean normalized frequency and average undulation associated with the family were calculated. These mean normalized frequencies and average undulations were then averaged across all the specimens in the group and the information gathered for each group was then compared with the other groups by age and genotype. This grouping of families

allowed for the easier analysis of statistical significance, which was calculated using two-way ANOVA with a post-hoc Tukey test in both GraphPad and MATLAB.

4.4 Results

When these distributions are analyzed in terms of collagen fiber families, an interesting result tends to arise. As is observed in **Figure 4.2**, for the wild-type (WT) specimens there is a but statistically significant increase in the relative number of circumferentially oriented fibers and a decrease in axially oriented fibers with age. Overall, this is slight accompanied by an expected decrease in collagen fiber tortuosity with increased age, though this fiber stiffening can be seen to a somewhat greater extent with the circumferential and helical fibers than with the axial fibers. When comparing the panels of **Figure 4.2**, one can ascertain the effects of both age and genotype on the orientation and tortuosity of the collagen fibers.

Observing the relative frequencies of the collagen fiber families of the WT mice with increasing age in **Figure 4.2a**, there is a clear difference between the relative frequencies of the axial and circumferential collagen families. At both 6 weeks and 3 months, there is a clear but statistically insignificant difference between the relative amounts of collagen fibers in the axial and circumferential fiber families, with a larger number of circumferential collagen fibers. As this group of mice age, there is no noticeable shift in the average normalized frequencies in either the axial or circumferential collagen fibers at 6 months and 12 months. At these ages, however, there is a significant difference between the mean normalized frequencies of the axial and circumferential fibers.

This change, or lack thereof, in collagen fiber frequencies is distinct from the results in the knockout (KO) mice in **Figure 4.2b**, where there is an overall increase in circumferential collagen fibers. In contrast to the wild-type mice of **Figure 4.2a**, the KO mice at 6 weeks have a greater frequency of axial collagen fibers. However, there is a much greater shift to increased circumferential collagen fibers with increasing age. Even though this difference is not statistically significant until the mice reach 12 months of age, the shift in the collagen fiber frequencies is much greater in the KO mice than in the WT mice. When isolating the frequency values at 12 months of age, there is a clear disparity in the differences between these two fiber families in the WT and KO mice.

While there is a clear trend in the evolution of collagen fiber frequencies with age for the KO but not for the WT mice, the tortuosity of the fibers do not show as clear of a distinction in overall remodeling between the two genotypes. As can be seen in **Figure 4.2c**, the decrease in the fiber tortuosity/undulation with age is greater within the circumferential family than in the axial family. While the 6-week WT mice have relatively similar undulations in both the axial and circumferential collagen families, the tortuosity in the circumferential direction steadily decreases in the first 6 months of age while the axial fiber tortuosity only undergoes a slight decrease. This decrease continues until the tortuosity of the circumferential collagen fibers is significantly less than that of the axial fibers in the 6-month group. Axial fiber tortuosity greatly decreases in the 12-month group. However, the circumferential fibers are still significantly less undulated than the axial fibers. The difference in the circumferential tortuosity between the 6-month and 12-month

group is far less than among the previous age groups, possibly suggesting less vascular remodeling in the older age groups of the WT genotype.

Compared to the WT group, the KO mice display slightly different trends in terms of their tortuosity with increasing age (**Figure 4.2d**). As in the WT mice in the previous panel, the tortuosity in the axial and circumferential directions is similar in young KO mice. Unlike the WT group, the average tortuosity of the axial fiber slightly increases in the KO mice, with very little change after 3 months. Also, while the average tortuosity of the circumferential fiber family decreases with time overall, it increases slightly but no significantly between the 3-month and 6-month groups. The standard error in tortuosity is too large to achieve statistically significant differences between groups. The only time point at which the two fiber families are statistically different is at 12 months, where the circumferential fibers are significantly less undulated than the axial fibers. When comparing the KO mice in this panel with the WT mice in the previous panel, the difference between the undulations of the two mentioned collagen fiber families is much greater compared to their WT counterparts. However, most of this is a result of a relative increase in the axial undulation rather than a greater decrease in that of the circumferential fiber family.

Figure 4.3 demonstrates an overall shift in fiber orientation toward the circumferential direction by isolating the trends in the frequencies of the circumferential fibers among the three studied genotypes (WT, KO, and HET). Here, there is a statistically significant shift observed in the KO mice where NO signaling is reduced compared to the other genotypes. As seen in this figure, there

is no significant difference among the amounts of circumferential collagen fibers until the mice reach 12 months of age. At this point, the KO mice have significantly more circumferential fibers than either the WT or the HET mice. Interestingly, there is no significant difference between the frequencies of the WT and the HET mice in any of the age groups. The WT mice undergo a small but steady increase in the relative frequency of the circumferential fibers until 6 months, at which point it levels out. In the HET mice, the average circumferential frequency reaches its maximum amount at 3 months before decreasing.

Overall, this shift in collagen fiber distribution toward the circumferential direction is amplified by the reduction in eNOS signaling as shown by the knockout distributions. This is accompanied by a sharper decrease in circumferential collagen fiber tortuosity. These general trends can also be observed from the data collected across all samples in **Table 4.1** and **Table 4.2**. While not displayed in either of the figures mentioned in this section, the changes in the relative normalized frequencies of the two helical families (**Table 4.1** and **Table 4.2**) account for some of the disparities in the frequencies of the axial and circumferential groups. For the future development of computational models, the mathematical parameters that define the Gaussian distributions derived from the collagen histograms are listed in **Figure 4.4** and **Table 4.3** for orientation and tortuosity, respectively.

4.5 Discussion

The main purpose of this study was to investigate the microstructural changes observed in murine aorta under ECD via an eNOS knockout model. The

orientation and tortuosity of the collagen fibers within each of the samples were successfully quantified via SHG analysis in terms of both distribution curves and frequency of fiber families. While previous clinical data has shown a tendency for blood vessels under ECD to undergo intimal-medial thickening because of collagen fiber deposition and, on occasion, smooth muscle expansion, very few studies have directly examined the changes in the collagen microstructure or have made inferences related to the resulting changes in mechanical properties.

Observing the trends depicted in **Figure 4.2**, the correlation between the change in collagen fiber direction and undulation/tortuosity and a lack of endothelial signaling begins to emerge. In terms of fiber orientation, the knockout specimens underwent a decrease in the number of axially oriented fibers and an increase in circumferentially oriented fibers with increasing age. This trend was not observed, however, in the wild-type mice. Although the differences between the frequency of these two families were significant at later ages (both 6 months and 12 months) in the wild-type mice (**Figure 4.2a**), the shift in collagen fiber orientation was more dramatic with age in the knockout mice (**Figure 4.2b**). As can be observed by the bolded numbers in **Table 4.1**, the differences in frequency between the axial and circumferential collagen fibers is greater in the knockout mice than in the wild-type mice.

One observation that is peculiar in the wild-type mice is the lack of change in orientation (**Figure 4.2a**), and undulation (**Figure 4.2c**) after 6 months. With orientation, there is very little change after 3 months, and even the change that occurred between 6 weeks and 3 months is very small. In terms of

undulation/tortuosity, there remains a steady decrease in the tortuosity of the circumferential fibers but there is negligible change going from 6 months to 12 months compared to the difference between the other age groups, as indicated by the slope of the line in the plot. While the trends observed in terms of tortuosity are not statistically significant, they may suggest that in the absence of disease (such as ECD), the elastic arteries are only able to remodel to a certain point purely because of age. Based on a computational model developed by Valentin, et al., this may occur at older ages if remodeling kinetic constants are very low [113]. However, most aging coincides with the development of ECD as a result of endothelial cell senescence, so this occurrence is very unlikely in practice [110].

This lack of remodeling in the older age groups is not observed, however, among the circumferential fibers in the knockout mice in terms of both orientation (**Figure 4.2b**) and tortuosity (**Figure 4.2d**). When looking at orientation, there is a consistent increase in the relative frequency of collagen fibers in the circumferential family coupled with a similar decline in that of the axial family. In contrast to the differences between these two families for the wild-type (WT) mice, the difference in the relative frequencies of the axial and circumferential collagen families in the knockout (KO) mice is significantly more pronounced.

Overall, these results are consistent with the physiological outcomes of ECD. Because the smooth muscle is unable to adapt to the increased circumferential stress brought about by increases in pressure, it makes sense that there is increased collagen deposition in the circumferential direction. The orientation of newly deposited collagen tends to be stress-mediated [111]. Because

pressure is translated to circumferential stress on a cylinder, one can assume that most of the newly deposited collagen will be oriented toward the circumferential direction [45]. As with the WT mice, the tortuosity of the circumferential fibers decreases with age. However, there is also an overall observed increase in the undulation of the axial collagen fibers. Because few studies have looked at the physiological significance of the remodeling of axial collagen in terms of tortuosity, this finding may open the door to future experimental and modeling studies concerning changes in mechanical properties and relationship with vascular disease and overall changes to the elastic arteries with age. For example, this may be related to the increased tortuosity of the aorta as a whole with age [9].

The increase in the frequency of circumferential collagen fibers is highlighted in **Figure 4.3**. As can be seen by the trends with age among the wild-type, heterozygous, and knockout specimens, the normalized frequencies of circumferential collagen fibers increase with age for almost all genotypes. The exception to this trend is seen in the HET mice, which reached a maximum relative number of circumferential fibers in the 3-month group before slowly decreasing with age. While the relative number of circumferential collagen fibers in the 6-week KO mice was less, they steadily increased over time while the other families only slightly increased. At 12 months of age the frequency of circumferential fibers in the knockout mice is significantly greater than in the heterozygous or the wild-type mice. Interestingly in **Figure 4.3**, there was not a significant difference between the WT and HET circumferential collagen frequencies at any age group. While more work needs to be accomplished, this observation indicates that a partial

genotype for vascular NO signaling may be sufficient for adequate endothelial functioning. Should these results be backed up by further investigation, it could have clinical implication in terms of the determination of adequate dosage for nitrates geared toward pharmaceutical NO administration.

While more research is required to find the mechanism behind this dramatic shift, one can hypothesize that this may be due to a greater demand in support from the arterial extracellular matrix to compensate for increases in blood pressure. Because vascular ECD implies a decreased flow-mediated vasodilation, the artery is less able to adjust to increases in pressure. Therefore, the arteries must become stronger to prevent the fracturing of the wall. As can be seen in **Table 4.3**, the average collagen angle for the 12-month knockout mice is closer to 90 degrees from the axial direction than any other age or genotype. However, most of the other parameters of the distribution curves tend to have a greater correlation with age than with genotype. Nonetheless, these Gaussian orientation distribution curves will allow for an accurate representation of the collagen orientation of each age and genotype in the development of future mechanical models of this disease.

Parameters for the Gaussian distribution curves for tortuosity can be seen in **Table 4.4**. In this table, it appears that tortuosity tends to have a greater correlation with age than with genotype, with tortuosity decreasing with increasing age. This shows that while ECD has a direct effect on the collagen deposition and fiber orientation, it does not affect the undulation at which the fibers are deposited. This indicates that even though there is a greater amount of collagen within arteries affected by this condition, the tissue can still be stretched by the same amount

before many of the collagen fibers become load bearing. This also challenges the previous assumption that ECD causes arteries to age more rapidly [104,110]. Rather, it appears that this disease causes the arteries to remodel into a material with its own unique mechanical properties. Therefore, the future experimental and computational study of vascular endothelial dysfunction, isolated from any corresponding conditions, is needed to gain a greater understanding of the effects this disease has on arterial mechanical properties.

4.6 Tables and Figures

Table 4.1. Mean Normalized Frequencies for Four Fiber Families

Mean Normalized Frequency						
Age	**Genotype**		**Axial**	**Circumferential**	**Helical 1**	**Helical 2**
6 weeks	Wild-Type	Average	0.196	0.290	0.273	0.242
		SD	0.129	0.130	0.145	0.147
	Heterozygous	Average	0.280	0.232	0.219	0.269
		SD	0.177	0.103	0.176	0.198
	Knockout	Average	0.321	0.188	0.230	0.261
		SD	0.180	0.149	0.169	0.128
3 months	Wild-Type	Average	0.193	0.326	0.297	0.185
		SD	0.183	0.166	0.170	0.100
	Heterozygous	Average	0.156	0.332	0.179	0.333
		SD	0.115	0.100	0.083	0.088
	Knockout	Average	0.182	0.323	0.331	0.164
		SD	0.103	0.137	0.136	0.096
6 months	Wild-Type	Average	0.195	0.321	0.287	0.197
		SD	0.098	0.075	0.104	0.103
	Heterozygous	Average	0.209	0.331	0.260	0.200
		SD	0.138	0.166	0.164	0.129
	Knockout	Average	0.143	0.352	0.280	0.225
		SD	0.087	0.116	0.149	0.157
12 months	Wild-Type	Average	**0.204**	**0.314**	0.212	0.284
		SD	0.129	0.101	0.098	0.116
	Heterozygous	Average	0.219	0.281	0.127	0.373
		SD	0.127	0.155	0.084	0.109
	Knockout	Average	**0.089**	**0.460**	0.209	0.242
		SD	0.013	0.030	0.105	0.097

Apart from the knockout samples, all differences in age for all fiber families were statistically significant ($p<0.05$). Differences among genotypes were also significant ($p<0.01$). The quantities in bold represent the twelve-month values indicated by the asterisks in **Figure 4.2**.

Table 4.2. Mean Tortuosity for Four Quadrants of Fiber Families.

Mean Tortuosity						
Age	**Genotype**		**Axial**	**Circumferential**	**Helical 1**	**Helical 2**
6 weeks	Wild-Type	Average	1.333	1.346	1.354	1.347
		SD	0.081	0.080	0.132	0.050
	Heterozygous	Average	1.320	1.296	1.361	1.342
		SD	0.063	0.008	0.063	0.085
	Knockout	Average	1.308	1.344	1.322	1.310
		SD	0.064	0.058	0.031	0.097
3 months	Wild-Type	Average	1.339	1.317	1.308	1.344
		SD	0.048	0.074	0.080	0.056
	Heterozygous	Average	1.382	1.306	1.370	1.320
		SD	0.118	0.046	0.109	0.034
	Knockout	Average	1.336	1.291	1.277	1.350
		SD	0.074	0.028	0.037	0.065
6 months	Wild-Type	Average	1.323	1.265	1.292	1.337
		SD	0.031	0.005	0.019	0.012
	Heterozygous	Average	1.316	1.274	1.353	1.324
		SD	0.073	0.108	0.160	0.105
	Knockout	Average	1.336	1.313	1.337	1.344
		SD	0.055	0.052	0.155	0.049
12 months	Wild-Type	Average	**1.290**	**1.261**	1.276	1.273
		SD	0.041	0.012	0.040	0.050
	Heterozygous	Average	1.291	1.267	1.367	1.275
		SD	0.074	0.054	0.103	0.042
	Knockout	Average	**1.339**	**1.252**	1.295	1.294
		SD	0.012	0.019	0.043	0.041

Apart from the wild-type samples, all differences in age for all fiber families were statistically significant ($p<0.05$). Differences among genotypes were also significant ($p<0.05$). The quantities in bold represent the points in **Figure 4.2** indicated by an asterisk.

Table 4.3. Collagen Fiber Undulation Curve Parameters

		Avg Tortuosity	SD	a1	b1	c1	a2	b2	c2
6 weeks	Wild-Type	1.258	0.038	8.276	-1.309	1.115	0.036	1.050	1.115
	Heterozygous	1.270	0.039	3.461	-0.782	0.968	0.044	1.048	0.017
	Knockout	1.261	0.049	14.730	-1.480	1.129	0.041	1.050	0.013
3 months	Wild-Type	1.288	0.066	2.034	-0.322	0.795	0.065	0.990	0.003
	Heterozygous	1.270	0.060	1.731	-0.613	0.963	0.053	1.047	0.028
	Knockout	1.244	0.017	1.166	-0.251	0.819	0.055	1.049	0.028
6 months	Wild-Type	1.251	0.001	2.723	-0.787	0.991	0.063	1.048	0.029
	Heterozygous	1.246	0.113	2.257	-0.313	0.775	0.062	1.052	0.020
	Knockout	1.252	0.027	0.942	-0.011	0.711	0.050	1.054	0.015
12 months	Wild-Type	1.217	0.063	1.126	-0.174	0.779	0.056	1.046	0.019
	Heterozygous	1.229	0.037	0.800	-0.052	0.750	0.068	1.048	0.025
	Knockout	1.226	0.024	5.488	-0.929	0.986	0.049	1.049	0.001

Parameters for the representative distribution curves of the collagen fiber tortuosity for each of the different groups along with the average tortuosity for each group, (SD= standard deviation). The characteristic equation for each of these terms corresponds to **Equation 1** where the summation only goes to i=2. Each of the terms a1, b1, c1, etc. represent the corresponding constants shown in **Equation 1**. All distributions used to get these representative curve parameters were fit to the Gaussian model with an $R^2 > 0.95$.

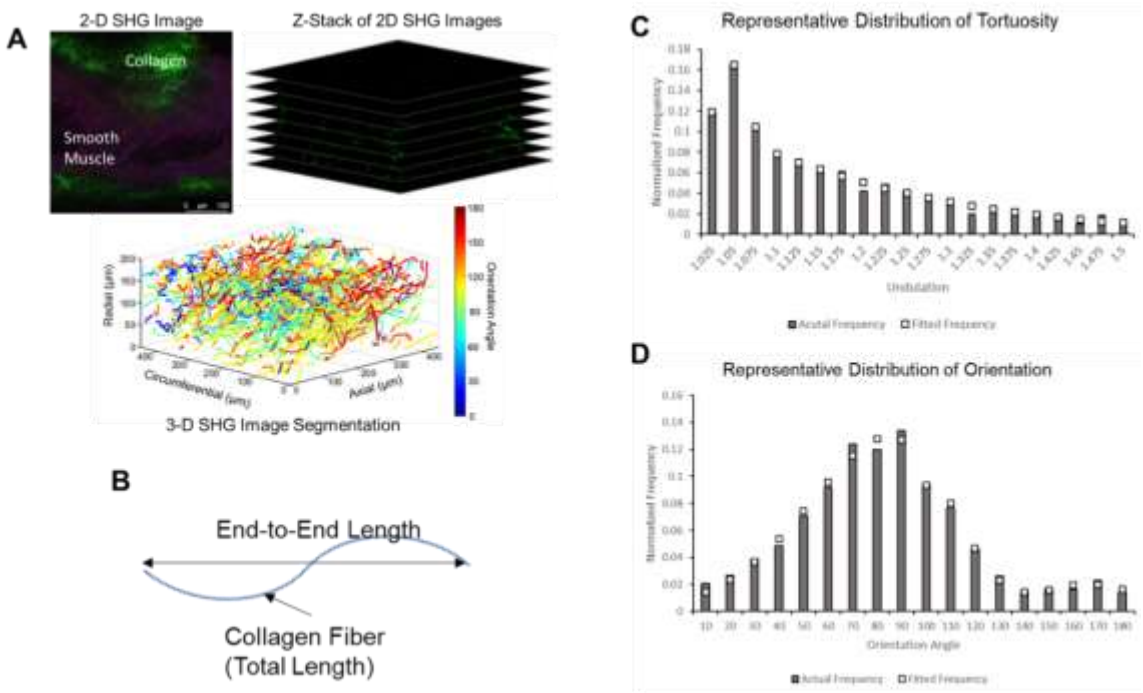

Figure 4.1. Illustration of image processing and histogram analysis for the creation of representative distribution curves for undulation and orientation. **A)** Depicted is a typical image obtained by SHG microscopy, followed by a typical z-stack of the images through the depth of the sample. Before the collagen fibers can be analyzed, the orientation of the smooth muscle cells (SMC) is determined to set the alignment of the axes. These fibers are then processed in a custom MATLAB program where they are reconstructed in a 3-D model to determine information regarding the orientation angle, elevation angle, and tortuosity. (*Get better image that shows only smooth muscle or only collagen, provide axis for orientation*) **B)** Representation for the measurements used to calculate tortuosity/undulation, where the end-to-end length represents the straight length between each ends of the fiber while the total length represents the length along all the curves of the fiber. **C)** Undulation histograms obtained from each specimen in a group are averaged and used to obtain a representative histogram for that group. A two-term Gaussian curve is then fitted to that representative histogram. **D)** Histograms of the collagen orientation angles for each specimen are used to create individual Gaussian distribution curves. The parameters from these curves are then averaged to create a representative distribution curve. (**A** was adapted from a figure created by William Torres)

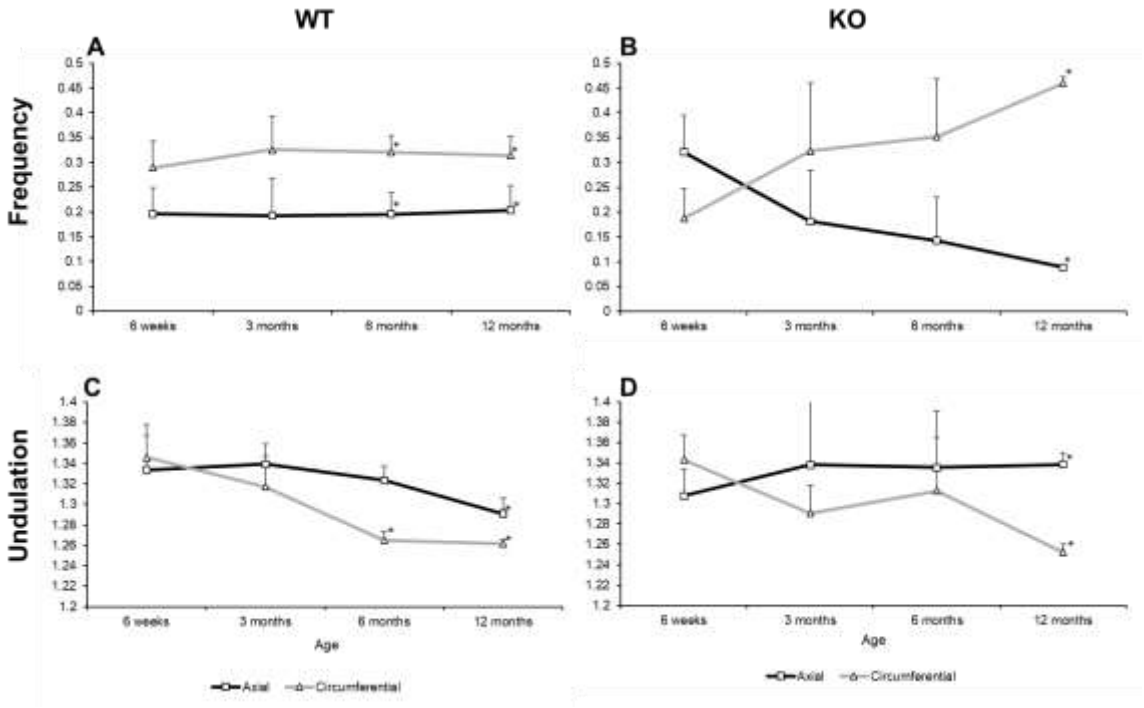

Figure 4.2. Representative results detailing the changes in collagen fiber distribution and tortuosity/undulation for wild-type and NOS knockout specimen groups with age. All error bars denote the standard error of the mean. **A)** Familial distributions of collagen fiber orientation for wild-type samples over age ($p<0.01$). **B)** Familial distributions for collagen fiber orientation for knockout samples with age ($p<0.001$). **C)** Average fiber tortuosity for each family with age for wild-type specimens ($p<0.05$), **D)** Average fiber tortuosity for each family with age for knockout specimens ($p<0.05$). Expanded results of this information are shown in **Table 4.1** and **Table 4.2**. Asterisks (*) on data points indicate areas in the data that are significantly different from their counterparts in the opposite fiber family.

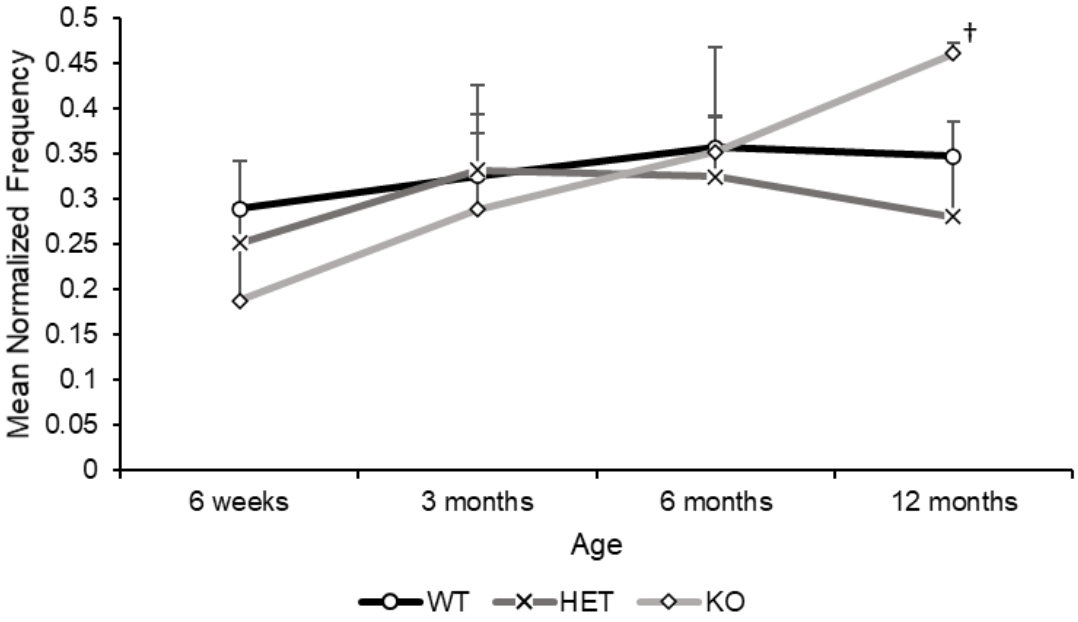

Figure 4.3. Depiction of the observed trends for the normalized distribution frequency for collagen fibers aligned in the circumferential direction for wild-type, heterozygous, and knockout samples. Error bars denote the positive standard error from the mean. Points marked with a dagger (†) indicate points that are significantly different from their counterparts in the other genotypes. Expanded results of this information are shown in **Table 4.1** and **Table 4.2** ($p<0.05$).

Age	Genotype		Average Angle	a1	b1	c1	a2	b2	c2	a3	b3	c3
6 weeks	Wild-type	Average	77.925	0.096	81.410	44.769	0.046	95.075	61.335	0.023	58.250	10.920
		SD	3.218	0.040	11.633	31.510	0.019	51.510	60.626	0.025	23.501	17.805
	Heterozygous	Average	106.326	0.244	114.275	59.835	0.122	113.648	25.466	-0.015	103.178	9.289
		SD	9.850	0.309	10.626	14.422	0.135	39.551	23.961	0.019	36.090	14.237
	Knockout	Average	97.765	0.238	117.662	51.935	0.084	58.917	26.758	0.041	90.646	38.354
		SD	12.301	0.170	113.822	39.294	0.049	60.029	12.557	0.028	71.358	48.111
3 months	Wild-type	Average	84.240	0.133	76.022	49.926	-0.049	114.978	113.715	0.014	103.850	30.964
		SD	15.379	0.050	18.868	14.270	0.070	93.105	202.426	0.031	21.752	39.733
	Heterozygous	Average	101.121	0.118	119.420	32.998	0.042	124.722	131.370	0.017	142.020	7.734
		SD	13.134	0.057	34.730	31.738	0.063	45.906	227.129	0.022	19.865	6.987
	Knockout	Average	72.551	0.126	-157.322	133.233	0.061	10.597	7.089	0.030	4.161	0.508
		SD	7.246	0.059	316.189	264.578	0.035	20.744	11.506	0.017	8.628	0.910
6 months	Wild-type	Average	87.954	0.074	-0.070	1.597	0.048	-1.372	0.301	0.035	-0.710	0.031
		SD	5.823	0.002	0.206	0.021	0.032	1.360	0.242	0.038	0.809	0.039
	Heterozygous	Average	86.390	0.183	0.035	0.375	0.077	-0.760	0.552	0.051	-0.148	0.567
		SD	22.865	0.145	1.105	0.427	0.013	0.798	0.543	0.023	0.663	0.576
	Knockout	Average	85.802	0.111	-0.056	0.830	0.039	-0.028	1.114	0.019	0.389	0.137
		SD	19.146	0.038	0.402	0.476	0.026	0.415	1.421	0.015	0.182	0.138
12 months	Wild-type	Average	94.846	0.259	0.218	0.695	0.048	-0.929	1.586	0.021	-2.102	0.639
		SD	13.874	0.398	0.559	0.419	0.017	1.256	1.614	0.025	3.746	1.200
	Heterozygous	Average	110.680	0.241	0.477	0.666	-0.069	0.790	1.390	0.042	1.095	0.227
		SD	16.269	0.255	0.761	0.632	0.337	1.496	0.984	0.035	0.724	0.176
	Knockout	Average	90.548	0.109	-0.182	0.505	0.152	0.149	0.924	0.032	-0.333	1.270
		SD	10.841	0.022	0.120	0.341	0.202	0.261	1.107	0.026	1.164	1.546

Figure 4.4. Parameters for the distribution curves of collagen fiber orientation for each of the different groups along with the average orientation angle relative to the axial direction, (SD= standard deviation). Each of the terms a1, b1, c1, etc. represent the corresponding constants shown in **Equation 1**. All distributions used to calculate these representative curve parameters were fit to the Gaussian model with an $R^2 > 0.90$.

Chapter 5

Conclusions and Future Directions

5.1 Conclusions

ECD is a vascular disease characterized by the lack of signaling, especially NO signaling, from the endothelium. Largely the result of high oxidative stress, this disease that is commonly associated with aging is often exacerbated by numerous factors commonly associated with the modern Western lifestyle such as smoking, diabetes, and lack of physical activity. There are also some links between the onset of ECD and hypertension and COVID-19. If left untreated through lifestyle changes, the progression of ECD can result in the onset of hypertension, aneurysm development, atherosclerosis, and future heart failure.

The presence of ECD is often associated with a change in physiological functioning and overall wall structure. Most notably, ECD is associated with a decrease in %FMD due to an inability of the vascular endothelium to respond to changes in blood flow. It is also associated with an increase in PWV, which is often an indicator of a decreased influence of the elastic lamina on mechanical behavior. This change in mechanical behavior is also seen through an increase in wall stiffness as observed by an increase in elastic modulus. Changes in the structure of the arteries is also seen in an increase in IMT, which is mostly a result of excessive collagen deposition with some smooth muscle proliferation.

While the physiological and histological outcomes of ECD are well documented, there remain few studies that have directly modeled the mechanical behavior of the artery after growth and remodeling caused by ECD. While phenomenological models will likely need to be used to provide a characteristic strain energy function from which one can develop an accurate stress-strain relationship, a structurally motivated growth and remodeling approach will be needed to provide the predictive value necessary for accurate modeling in the future. To this end, kinematic relationships must be defined for the undeformed, deformed, and remodeled states for the body and the individual constituents. Then the individual constituents must be given strain energy equations to characterize their individual mechanical behavior, from which collagen must be assigned as a complex matrix of fibers with a distribution of orientations. Lastly, kinetic G&R parameters must be assigned to characterize the time-dependent remodeling of constituent configurations. Previous studies that have developed models of similar disease states show an overall change in physiological functioning with an increased wall stiffness. These models can be useful if they are modified to account for the nuances of changes resulting from reduced NO signaling. Other studies have examined maladaptive remodeling that arise from sustained increase in flow rate, in which arterial wall thickening, increased collagen deposition, and increased wall stiffness are observed. These models can be useful if they are modified such that there is a lessened contribution of vasoactive dilation to mechanical behavior.

Overall, the experimental studies tend to confirm and expand upon the conclusions gathered from the literature review. In our experiments, mouse aortic specimens gathered from WT, KO, and HET groups were successfully imaged using SHG microscopy. Based on analysis from the gathered images, a set of conclusions can be gathered on the effects of endothelial dysfunction on the microstructure of the vascular wall. Overall, our previously stated initial hypothesis was proved by our experimental evidence. It was observed that mice with vascular endothelial dysfunction (KO) have a much greater relative number of fibers oriented in the circumferential direction. Interestingly, partial endothelial nitric oxide signaling, as demonstrated by the HET mice, also has no noticeable effect on the vascular microstructure compared to those with normal signaling. On the other hand, while tortuosity remains similar for mice both with and without ECD (both WT and KO mice), there is a slight increase in the tortuosity of the axial fibers in the knockout mice.

5.2 Future Directions

With the background in knowledge regarding ECD provided in this thesis, future research efforts pertaining to this disease may be inspired. One area of such future research could investigate the effects of ECD on the microstructure and mechanical properties of the arterial wall. However, studies conducted in this area must aim to isolate effects caused by inadequate NO bioavailability from conditions with which it is normally coupled, such as hypertension, atherosclerosis, and aging. Therefore, future mechanical models should focus on using the common effects of the diseases associated with ECD along with data derived from animal models of

disease to conclude the associated biological phenomena and adapt their models accordingly. From there, the increased complexity and nuance derived from further study of the vascular extracellular matrix can be added to gain a more complete description of the microstructurally derived mechanical properties.

With this current experiment, we lacked the ability to gather complete histological data of the aortas from the mice used to model ECD. For each age and genotype, murine aortas are extracted like is done in the previous chapter, stained with Picrosirius Red, and fixated in paraffin before being analyzed under light microscopy. Using custom image analysis software, the relative collagen content was calculated via the area fraction of the stain. A current but incomplete data set is shown in **Figure 5.1**. Currently, the KO mice display an expected increase in the area fraction of collagen with age. This data set is almost complete with only a few data points missing. While this trend is not yet observed in the WT and HET mice, most of these age groups only contain one or two data points which are not representative of the entire sample. Based on the literature review one should expect the collagen area fraction to increase with age in all mice, with the WT and HET mice displaying a lower area fraction overall compared to the KO mice but most notably in the younger mice. This data may be incomplete, but its completion is paramount in being able to use changes in microstructural content as a justification for observed changes in the mechanical properties of the arterial wall.

Future experimental studies may look toward gaining a deeper understanding of the mechanical properties of arteries affected by ECD. While

there have been numerous experimental studies detailing the properties of these arteries in-vivo, very few studies have characterized them through uniaxial or biaxial inflation-extension testing. By doing these tests and gaining stress and strain data, one can come to a better understanding of the mechanical nature of the arterial wall [93,131]. In the translation of experimental data into a mathematical platform, such direct mechanical data can be used to supplement the previously discussed clinical data to obtain an accurate computational model of the dysfunctional arterial wall [59].

Another area of future direction is through the development of a mechanical model based on observed microstructural data. According to the experimental data, a common trend among subjects with vascular ECD is intimal-medial thickening derived from collagen expansion coupled with gradual elastin degradation [7,88]. Because collagen growth tends to adapt to the residual pre-stress, one may assume that a lack of vasoactive dilation would cause an increase in circumferential collagen [24,87]. While, experimental data has yet to confirm this finding in ECD, preliminary models may take the approach of forcing newly deposited collagen to follow a distribution with a circumferential mode while implementing a uniform decay function for elastin [50,126]. Another approach would be through the four fiber family model, in which the circumferential collagen family would have a continuous growth with age [84]. However, true collagen growth rates and distributions must be confirmed with experimental evidence before implementation into a mathematical model.

Pathways for further development also include a predictive, NO-coupled mathematical formulation of vascular growth and remodeling. Even though a mechanical model based on local chemical concentrations would normally interfere with the assumption of a continuum, evidence suggests a functional relationship between NO bioavailability and medial collagen synthesis [56,73]. While this exact relationship has yet to be mathematically quantified, such an experimental study would be critical in directly linking NO and maladaptive growth and remodeling. Such a direct link would allow for the transformation of clinical and experimental data of nitric oxide bioavailability into a growth and remodeling framework from which a continuum mechanics model can be developed. Because age and hypertension-related collagen deposition models of growth and remodeling have already been established, one can easily translate these models into an ECD model with a NO-dependent synthesis of collagen with a prescribed distribution [84,113].

5.3 Tables and Figures

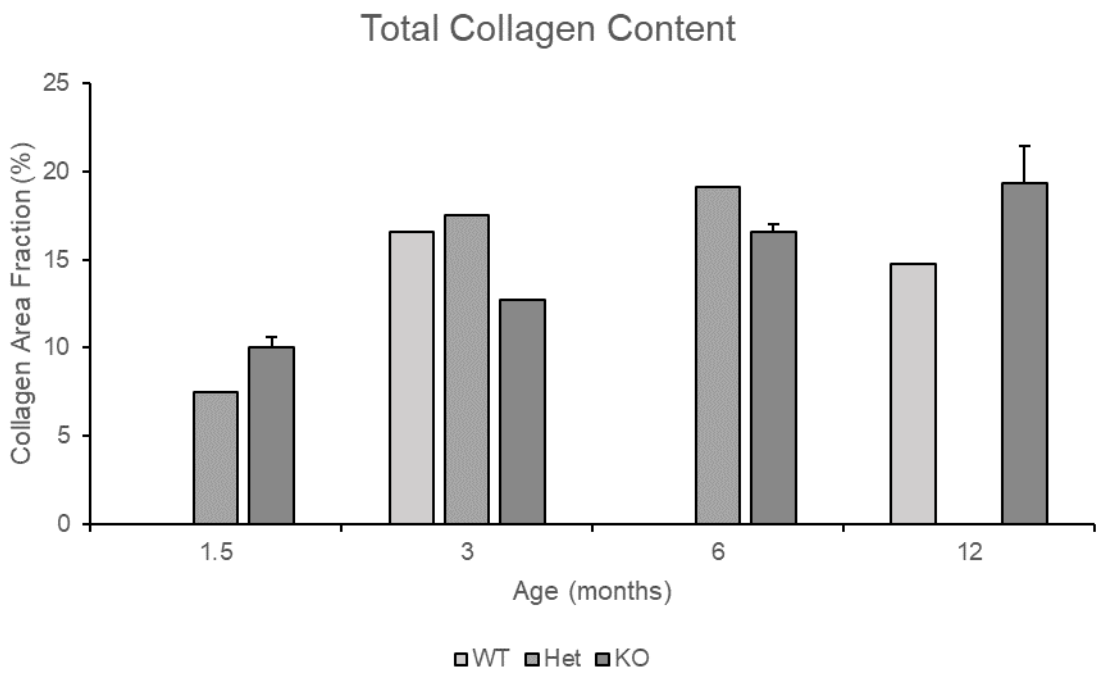

Figure 5.1. Total collagen content in each group of mice as measured by area fraction. Error bars represent the standard error of the mean (SEM) and are only applied to groups that contain more than two samples. (Histology data acquired and compiled by Liya Du)

References

1. Alford, P. W., J. D. Humphrey, and L. A. Taber. Growth and remodeling in a thick-walled artery model: Effects of spatial variations in wall constituents. *Biomech. Model. Mechanobiol.* , 2008.doi:10.1007/s10237-007-0101-2

2. Amraei, R., and N. Rahimi. COVID-19, Renin-Angiotensin System and Endothelial Dysfunction. , 2020.doi:10.3390/cells9071652

3. Anderson, T. J. Arterial stiffness or endothelial dysfunctin as a surrogate marker of vascular risk. , 2006.doi:10.1016/s0828-282x(06)70990-4

4. Anghelescu, M., J. R. Tonniges, E. Calomeni, P. E. Shamhart, G. Agarwal, K. J. Gooch, and A. J. Trask. Vascular Mechanics in Decellularized Aortas and Coronary Resistance Microvessels in Type 2 Diabetic db/db Mice. *Ann. Biomed. Eng.* , 2015.doi:10.1007/s10439-015-1333-4

5. Azeloglu, E. U., M. B. Albro, V. A. Thimmappa, G. A. Ateshian, and K. D. Costa. Heterogeneous transmural proteoglycan distribution provides a mechanism for regulating residual stresses in the aorta. *Am. J. Physiol. - Hear. Circ. Physiol.* , 2008.doi:10.1152/ajpheart.01027.2007

6. Bank, A. J., and D. R. Kaiser. Smooth muscle relaxation: Effects on arterial compliance, distensibility, elastic modulus, and pulse wave velocity. , 1998.doi:10.1161/01.HYP.32.2.356

7. Beck, L., J. Su, S. Comerma-Steffensen, E. Pinilla, R. Carlsson, R. Hernanz, M. Sheykhzade, C. C. Danielsen, and U. Simonsen. Endothelial Dysfunction and Passive Changes in the Aorta and Coronary Arteries of Diabetic db/db Mice. *Front. Physiol.* , 2020.doi:10.3389/fphys.2020.00667

8. Bellini, C., J. Ferruzzi, S. Roccabianca, E. S. Di Martino, and J. D. Humphrey. A microstructurally motivated model of arterial wall mechanics with mechanobiological implications. *Ann. Biomed. Eng.* , 2014.doi:10.1007/s10439-013-0928-x

9. Belvroy, V. M., H. W. L. De Beaufort, J. A. Van Herwaarden, J. Bismuth, F. L. Moll, and S. Trimarchi. Tortuosity of the descending thoracic aorta: Normal values by age. *PLoS One* 14:1–12, 2019.

10. Bhattacharjee, R., J. Kim, W. H. Alotaibi, L. Kheirandish-Gozal, O. S. Capdevila, and D. Gozal. Endothelial dysfunction in children without hypertension: Potential contributions of obesity and obstructive sleep apnea. *Chest* , 2012.doi:10.1378/chest.11-1777

11. Van Bortel, L. M., M. J. Kool, and H. A. Struijker Boudier. Effects of antihypertensive agents on local arterial distensibility and compliance. , 1995.doi:10.1161/01.HYP.26.3.531

12. Braeu, F. A., A. Seitz, R. C. Aydin, and C. J. Cyron. Homogenized constrained mixture models for anisotropic volumetric growth and remodeling. *Biomech. Model. Mechanobiol.* , 2017.doi:10.1007/s10237-016-0859-1

13. Brandes, R. P., and J. Kreuzer. Vascular NADPH oxidases: Molecular mechanisms of activation. , 2005.doi:10.1016/j.cardiores.2004.08.007

14. Van Bussel, B. C. T., R. M. A. Henry, C. G. Schalkwijk, J. M. Dekker, G. Nijpels, and C. D. A. Stehouwer. Low-grade inflammation, but not endothelial dysfunction, is associated with greater carotid stiffness in the elderly: The Hoorn Study. *J. Hypertens.* , 2012.doi:10.1097/HJH.0b013e328350a487

15. Van Bussel, B. C., F. Schouten, R. M. Henry, C. G. Schalkwijk, M. R. De Boer, I. Ferreira, Y. M. Smulders, J. W. Twisk, and C. D. Stehouwer. Endothelial dysfunction and low-grade inflammation are associated with greater arterial stiffness over a 6-year period. *Hypertension* , 2011.doi:10.1161/HYPERTENSIONAHA.111.174557

16. Carlson, B. E., and T. W. Secomb. A theoretical model for the myogenic response based on the length-tension characteristics of vascular smooth muscle. *Microcirculation* , 2005.doi:10.1080/10739680590934745

17. Cecelja, M., and P. Chowienczyk. Role of arterial stiffness in cardiovascular disease. *JRSM Cardiovasc. Dis.* , 2012.doi:10.1258/cvd.2012.012016

18. Chiu, J. J., S. Usami, and S. Chien. Vascular endothelial responses to altered shear stress: Pathologic implications for atherosclerosis. , 2009.doi:10.1080/07853890802186921

19. Cho, J. G., A. Lee, W. Chang, M. S. Lee, and J. Kim. Endothelial to mesenchymal transition represents a key link in the interaction between inflammation and endothelial dysfunction. , 2018.doi:10.3389/fimmu.2018.00294

20. Cocciolone, A. J., J. Z. Hawes, M. C. Staiculescu, E. O. Johnson, M. Murshed, and J. E. Wagenseil. Elastin, arterial mechanics, and cardiovascular disease. , 2018.doi:10.1152/ajpheart.00087.2018

21. Cunningham, K. S., and A. I. Gotlieb. The role of shear stress in the pathogenesis of atherosclerosis. , 2005.doi:10.1038/labinvest.3700215

22. Cyron, C. J., R. C. Aydin, and J. D. Humphrey. A homogenized constrained mixture (and mechanical analog) model for growth and remodeling of soft tissue. *Biomech. Model. Mechanobiol.* , 2016.doi:10.1007/s10237-016-0770-9

23. Desyatova, A., J. MacTaggart, and A. Kamenskiy. Constitutive modeling of human femoropopliteal artery biaxial stiffening due to aging and diabetes. *Acta Biomater.* , 2017.doi:10.1016/j.actbio.2017.09.042

24. Driessen, N. J. B., W. Wilson, C. V. C. Bouten, and F. P. T. Baaijens. A computational model for collagen fibre remodelling in the arterial wall. *J. Theor. Biol.* , 2004.doi:10.1016/j.jtbi.2003.08.004

25. Eberth, J. F., L. Cardamone, and J. D. Humphrey. Evolving biaxial mechanical properties of mouse carotid arteries in hypertension. *J. Biomech.* , 2011.doi:10.1016/j.jbiomech.2011.07.018

26. Epstein, F. H., S. Moncada, and A. Higgs. The L-Arginine-Nitric Oxide Pathway. *N. Engl. J. Med.* , 1993.doi:10.1056/nejm199312303292706

27. Fleenor, B. S. Large elastic artery stiffness with aging: Novel translational mechanisms and interventions. , 2013.

28. Förstermann, U., and W. C. Sessa. Nitric oxide synthases: Regulation and function. *Eur. Heart J.* 33:829–837, 2012.

29. Gade, P. S., A. M. Robertson, and C. Y. Chuang. Multiphoton Imaging of Collagen, Elastin, and Calcification in Intact Soft-Tissue Samples. *Curr. Protoc. Cytom.* , 2019.doi:10.1002/cpcy.51

30. Gavriilaki, E., P. Anyfanti, M. Gavriilaki, A. Lazaridis, S. Douma, and E. Gkaliagkousi. Endothelial Dysfunction in COVID-19: Lessons Learned from Coronaviruses. , 2020.doi:10.1007/s11906-020-01078-6

31. Ghiadoni, L., S. Taddei, and A. Virdis. Hypertension and Endothelial Dysfunction: Therapeutic Approach. *Curr. Vasc. Pharmacol.* , 2011.doi:10.2174/157016112798829823

32. Gleason, R. L., and J. D. Humphrey. A 2D constrained mixture model for arterial adaptations to large changes in flow, pressure and axial stretch. *Math. Med. Biol.* , 2005.doi:10.1093/imammb/dqi014

33. Gokce, N., J. F. Keaney, L. M. Hunter, M. T. Watkins, Z. S. Nedeljkovic, J. O. Menzoian, and J. A. Vita. Predictive value of noninvasively determined endothelial dysfunction for long-term cardiovascular events in patients with peripheral vascular disease. *J. Am. Coll. Cardiol.* , 2003.doi:10.1016/S0735-1097(03)00333-4

34. Gori, T., J. D. Parker, and T. Mnzel. Flow-mediated constriction: Further insight into a new measure of vascular function. , 2011.doi:10.1093/eurheartj/ehq412

35. Granger, D. N., and P. R. Kvietys. Reperfusion injury and reactive oxygen species: The evolution of a concept. *Redox Biol.* 6:524–551, 2015.

36. Green, D. J., H. Jones, D. Thijssen, N. T. Cable, and G. Atkinson. Flow-mediated dilation and cardiovascular event prediction: Does nitric oxide matter? *Hypertension* , 2011.doi:10.1161/HYPERTENSIONAHA.110.167015

37. Hansen, L., I. Parker, R. L. Sutliff, M. O. Platt, and R. L. Gleason. Endothelial dysfunction, arterial stiffening, and intima-media thickening in large arteries from HIV-1 transgenic mice. *Ann. Biomed. Eng.* , 2013.doi:10.1007/s10439-012-0702-5

38. Harrison, M., K. Parkhurst, T. Tarumi, H. F. Lin, and H. Tanaka. Low flow-mediated constriction: Prevalence, impact and physiological determinant. *Clin. Physiol. Funct. Imaging* 31:394–398, 2011.

39. Heil, M., and A. L. Hazel. Fluid-structure interaction in internal physiological flows. *Annu. Rev. Fluid Mech.* , 2011.doi:10.1146/annurev-fluid-122109-160703

40. Higashi, Y., Y. Kihara, and K. Noma. Endothelial dysfunction and hypertension in aging. , 2012.doi:10.1038/hr.2012.138

41. Hoefer, I. E., B. Den Adel, and M. J. A. P. Daemen. Biomechanical factors as triggers of vascular growth. , 2013.doi:10.1093/cvr/cvt089

42. Holzapfel, G. A., and H. W. Weizsäcker. Biomechanical behavior of the arterial wall and its numerical characterization. , 1998.doi:10.1016/S0010-4825(98)00022-5

43. Huang, A., D. Sun, C. J. Smith, J. A. Connetta, E. G. Shesely, A. Koller, and G. Kaley. In eNOS knockout mice skeletal muscle arteriolar dilation to acetylcholine is mediated by EDHF. *Am. J. Physiol. - Hear. Circ. Physiol.* , 2000.doi:10.1152/ajpheart.2000.278.3.h762

44. Huang, C., and R. Ogawa. The link between hypertension and pathological scarring: Does hypertension cause or promote keloid and hypertrophic scar pathogenesis? *Wound Repair Regen.* , 2014.doi:10.1111/wrr.12197

45. Humphrey, J. D. Mechanisms of arterial remodeling in hypertension coupled roles of wall shear and intramural stress. , 2008.doi:10.1161/HYPERTENSIONAHA.107.103440

46. Humphrey, J. D., and K. R. Rajagopal. A constrained mixture model for arterial adaptations to a sustained step change in blood flow. *Biomech. Model. Mechanobiol.* , 2003.doi:10.1007/s10237-003-0033-4

47. Humphrey, J., and M. Epstein. Cardiovascular Solid Mechanics: Cells, Tissues, and Organs. *Appl. Mech. Rev.* , 2002.doi:10.1115/1.1497492

48. Jenkins, C., A. Milsted, K. Doane, G. Meszaros, J. Toot, and D. Ely. A cell culture model using rat coronary artery adventitial fibroblasts to measure collagen production. *BMC Cardiovasc. Disord.* , 2007.doi:10.1186/1471-2261-7-13

49. Jung, S. M., S. Jandu, J. Steppan, A. Belkin, S. S. An, A. Pak, E. Y. Choi, D. Nyhan, M. Butlin, K. Viegas, A. Avolio, D. E. Berkowitz, and L. Santhanam. Increased tissue transglutaminase activity contributes to central vascular stiffness in eNOS knockout mice. *Am. J. Physiol. - Hear. Circ. Physiol.* , 2013.doi:10.1152/ajpheart.00103.2013

50. Kapeliotis, M., R. A. Gavrila Laic, A. J. Peñas, J. Vander Sloten, P. Vanden Berghe, N. Famaey, and B. Depreitere. Collagen fibre orientation in human bridging veins. *Biomech. Model. Mechanobiol.* , 2020.doi:10.1007/s10237-020-01349-w

51. Karšaj, I., and J. D. Humphrey. A multilayered wall model of arterial growth and remodeling. *Mech. Mater.* , 2012.doi:10.1016/j.mechmat.2011.05.006

52. Karšaj, I., J. Sorić, and J. D. Humphrey. A 3-D framework for arterial growth and remodeling in response to altered hemodynamics. *Int. J. Eng. Sci.* 48:1357–1372, 2010.

53. Keshavarzian, M., C. A. Meyer, and H. N. Hayenga. Mechanobiological model of arterial growth and remodeling. *Biomech. Model. Mechanobiol.* , 2018.doi:10.1007/s10237-017-0946-y

54. Kim, J., and J. E. Wagenseil. Bio-Chemo-Mechanical Models of Vascular Mechanics. *Ann. Biomed. Eng.* , 2015.doi:10.1007/s10439-014-1201-7

55. Kleinbongard, P., A. Dejam, T. Lauer, T. Jax, S. Kerber, P. Gharini, J. Balzer, R. B. Zotz, R. E. Scharf, R. Willers, A. N. Schechter, M. Feelisch, and M. Kelm. Plasma nitrite concentrations reflect the degree of endothelial dysfunction in humans. *Free Radic. Biol. Med.* , 2006.doi:10.1016/j.freeradbiomed.2005.08.025

56. Kolpakov, V., D. Gordon, and T. J. Kulik. Nitric oxide-generating compounds inhibit total protein and collagen synthesis in cultured vascular smooth muscle cells. *Circ. Res.* , 1995.doi:10.1161/01.res.76.2.305

57. Korkmaz, H., and O. Onalan. Evaluation of endothelial dysfunction: Flow-mediated dilation. , 2008.doi:10.1080/10623320802228872

58. Kostelnik, C. J., K. J. Crouse, W. Carver, and J. F. Eberth. Longitudinal histomechanical heterogeneity of the internal thoracic artery. *J. Mech. Behav. Biomed. Mater.* 116:104314, 2021.

59. Kuhl, E., R. Maas, G. Himpel, and A. Menzel. Computational modeling of arterial wall growth. *Biomech. Model. Mechanobiol.* , 2007.doi:10.1007/s10237-006-0062-x

60. Latorre, M., and J. D. Humphrey. A mechanobiologically equilibrated constrained mixture model for growth and remodeling of soft tissues. , 2018.doi:10.1002/zamm.201700302

61. Leloup, A. J. A., C. E. Van Hove, S. De Moudt, G. W. De Keulenaer, and P. Fransen. Ex vivo aortic stiffness in mice with different eNOS activity. *Am. J. Physiol. Heart Circ. Physiol.* , 2020.doi:10.1152/ajpheart.00737.2019

62. Lessiani, G., F. Santilli, A. Boccatonda, P. Iodice, R. Liani, R. Tripaldi, R. Saggini, and G. Davì. Arterial stiffness and sedentary lifestyle: Role of oxidative stress. *Vascul. Pharmacol.* , 2016.doi:10.1016/j.vph.2015.05.017

63. Liao, J., and J. Farmer. Arterial stiffness as a risk factor for coronary artery disease. *Curr. Atheroscler. Rep.* , 2014.doi:10.1007/s11883-013-0387-8

64. Libby, P., and T. Lüscher. COVID-19 is, in the end, an endothelial disease. , 2020.doi:10.1093/eurheartj/ehaa623

65. Machyshyn, I. M., P. H. M. Bovendeerd, A. A. F. Van De Ven, P. M. J. Rongen, and F. N. Van De Vosse. A model for arterial adaptation combining microstructural collagen remodeling and 3D tissue growth. *Biomech. Model. Mechanobiol.* , 2010.doi:10.1007/s10237-010-0204-z

66. Marti, C. N., M. Gheorghiade, A. P. Kalogeropoulos, V. V. Georgiopoulou, A. A. Quyyumi, and J. Butler. Endothelial dysfunction, arterial stiffness, and heart failure. , 2012.doi:10.1016/j.jacc.2011.11.082

67. Mattson, J. M., R. Turcotte, and Y. Zhang. Glycosaminoglycans contribute to extracellular matrix fiber recruitment and arterial wall mechanics. *Biomech. Model. Mechanobiol.* , 2017.doi:10.1007/s10237-016-0811-4

68. McEniery, C. M., S. Wallace, I. S. MacKenzie, B. McDonnell, D. E. Newby, J. R. Cockcroft, and I. B. Wilkinson. Endothelial function is associated with pulse pressure, pulse wave velocity, and augmentation index in healthy humans. *Hypertension* 48:602–608, 2006.

69. Messner, B., and D. Bernhard. Smoking and cardiovascular disease: Mechanisms of endothelial dysfunction and early atherogenesis. , 2014.doi:10.1161/ATVBAHA.113.300156

70. Mordi, I., N. Mordi, C. Delles, and N. Tzemos. Endothelial dysfunction in human essential hypertension. , 2016.doi:10.1097/HJH.0000000000000965

71. Mullershausen, F., A. Lange, E. Mergia, A. Friebe, and D. Koesling. Desensitization of NO/cGMP signaling in smooth muscle: Blood vessels versus airways. *Mol. Pharmacol.* , 2006.doi:10.1124/mol.105.020909

72. Münzel, T., C. Sinning, F. Post, A. Warnholtz, and E. Schulz. Pathophysiology, diagnosis and prognostic implications of endothelial dysfunction. , 2008.doi:10.1080/07853890701854702

73. Myers, P. R., and M. A. Tanner. Vascular endothelial cell regulation of extracellular matrix collagen: Role of nitric oxide. *Arterioscler. Thromb. Vasc. Biol.* , 1998.doi:10.1161/01.ATV.18.5.717

74. Nägele, M. P., B. Haubner, F. C. Tanner, F. Ruschitzka, and A. J. Flammer. Endothelial dysfunction in COVID-19: Current findings and therapeutic implications. , 2020.doi:10.1016/j.atherosclerosis.2020.10.014

75. Neves, M. F., D. A. B. Kasal, A. R. Cunha, and F. Medeiros. Vascular dysfunction as target organ damage in animal models of hypertension. , 2012.doi:10.1155/2012/187526

76. Nichols, W. W., and D. G. Edwards. Arterial elastance and wave reflection augmentation of systolic blood pressure: Deleterious effects and implications for therapy. , 2001.doi:10.1177/107424840100600102

77. Nürnberger, J., A. Keflioglu-Scheiber, A. M. Opazo Saez, R. R. Wenzel, T. Philipp, and R. F. Schäfers. Augmentation index is associated with cardiovascular risk. *J. Hypertens.* , 2002.doi:10.1097/00004872-200212000-00020

78. Perticone, F., R. Ceravolo, A. Pujia, G. Ventura, S. Iacopino, A. Scozzafava, A. Ferraro, M. Chello, P. Mastroroberto, P. Verdecchia, and G. Schillaci. Prognostic significance of endothelial dysfunction in hypertensive patients. *Circulation* , 2001.doi:10.1161/01.CIR.104.2.191

79. Poggianti, E., L. Venneri, V. Chubuchny, Z. Jambrik, L. A. Baroncini, and E. Picano. Aortic valve sclerosis is associated with systemic endothelial dysfunction. *J. Am. Coll. Cardiol.* , 2003.doi:10.1016/S0735-1097(02)02622-0

80. Poredoš, P., M. Orehek, and E. Tratnik. Smoking is associated with dose-related increase of intima-media thickness and endothelial dysfunction. *Angiology* , 1999.doi:10.1177/000331979905000304

81. Quek, K. J., R. Boyd, O. Z. Ameer, B. Zangerl, M. Butlin, T. V. Murphy, A. P. Avolio, and J. K. Phillips. Progressive vascular remodelling, endothelial dysfunction and stiffness in mesenteric resistance arteries in a rodent model of chronic kidney disease. *Vascul. Pharmacol.* , 2016.doi:10.1016/j.vph.2015.12.004

82. Rachev, A. A model of arterial adaptation to alterations in blood flow. *J. Elast.* , 2000.doi:10.1023/A:1010800703478

83. Rachev, A., and T. Shazly. A structure-based constitutive model of arterial tissue considering individual natural configurations of elastin and collagen. *J. Mech. Behav. Biomed. Mater.* , 2019.doi:10.1016/j.jmbbm.2018.09.047

84. Rachev, A., and T. Shazly. A Two-Dimensional Model of Hypertension-Induced Arterial Remodeling With Account for Stress Interaction Between Elastin and Collagen. *J. Biomech. Eng.* , 2020.doi:10.1115/1.4045116

85. Rizzoni, D., E. Porteri, M. Castellano, G. Bettoni, M. L. Muiesan, G. Tiberio, S. M. Giulini, G. Rossi, G. Bernini, and E. Agabiti-Rosei. Endothelial

Dysfunction in Hypertension Is Independent From the Etiology and From Vascular Structure. *Hypertension* , 1998.doi:10.1161/01.HYP.31.1.335

86. Robertson, A. M., and P. N. Watton. Mechanobiology of the Arterial Wall. In: Transport in Biological Media. 2013.doi:10.1016/B978-0-12-415824-5.00008-4

87. Robertson, C., K. Ikemura, T. B. Krasieva, and S. C. George. Multiscale analysis of collagen microstructure with generalized image correlation spectroscopy and the detection of tissue prestress. *Biomaterials* , 2013.doi:10.1016/j.biomaterials.2013.04.019

88. Rudic, R. D., E. G. Shesely, N. Maeda, O. Smithies, S. S. Segal, and W. C. Sessa. Direct evidence for the importance of endothelium-derived nitric oxide in vascular remodeling. *J. Clin. Invest.* , 1998.doi:10.1172/JCI1699

89. Sáez, P., E. Peña, J. M. Tarbell, and M. A. Martínez. Computational model of collagen turnover in carotid arteries during hypertension. *Int. j. numer. method. biomed. eng.* , 2015.doi:10.1002/cnm.2705

90. Sakai, Y., H. Taki, and H. Kanai. Accurate evaluation of viscoelasticity of radial artery wall during flow-mediated dilation in ultrasound measurement. , 2016.doi:10.7567/JJAP.55.07KF11

91. Schulz, E., T. Gori, and T. Münzel. Oxidative stress and endothelial dysfunction in hypertension. , 2011.doi:10.1038/hr.2011.39

92. Selzer, F., K. Sutton-Tyrrell, S. Fitzgerald, R. Tracy, L. Kuller, and S. Manzi. Vascular stiffness in women with systemic lupus erythematosus. *Hypertension* , 2001.doi:10.1161/01.HYP.37.4.1075

93. Shazly, T., A. Rachev, S. Lessner, W. S. Argraves, J. Ferdous, B. Zhou, A. M. Moreira, and M. Sutton. On the Uniaxial Ring Test of Tissue Engineered Constructs. *Exp. Mech.* , 2015.doi:10.1007/s11340-014-9910-2

94. Sheinberg, D. L., D. J. Mccarthy, O. Elwardany, J. P. Bryant, E. Luther, S. H. Chen, J. W. Thompson, and R. M. Starke. Endothelial dysfunction in cerebral aneurysms. *Neurosurg. Focus* , 2019.doi:10.3171/2019.4.FOCUS19221

95. Siasos, G., K. Mourouzis, E. Oikonomou, S. Tsalamandris, V. Tsigkou, K. Vlasis, M. Vavuranakis, T. Zografos, S. Dimitropoulos, T. Papaioannou, A. Kalampogias, C. Stefanadis, A. Papavassiliou, and D. Tousoulis. The Role of Endothelial Dysfunction in Aortic Aneurysms. *Curr. Pharm. Des.* , 2015.doi:10.2174/1381612821666150826094156

96. Sitia, S., L. Tomasoni, F. Atzeni, G. Ambrosio, C. Cordiano, A. Catapano, S. Tramontana, F. Perticone, P. Naccarato, P. Camici, E. Picano, L. Cortigiani, M. Bevilacqua, L. Milazzo, D. Cusi, C. Barlassina, P. Sarzi-Puttini, and M. Turiel. From endothelial dysfunction to atherosclerosis. , 2010.doi:10.1016/j.autrev.2010.07.016

97. South, A. M., D. I. Diz, and M. C. Chappell. COVID-19, ACE2, and the cardiovascular consequences. , 2020.doi:10.1152/AJPHEART.00217.2020

98. Spronck, B., R. T. A. Megens, K. D. Reesink, and T. Delhaas. A method for three-dimensional quantification of vascular smooth muscle orientation: application in viable murine carotid arteries. *Biomech. Model. Mechanobiol.* , 2016.doi:10.1007/s10237-015-0699-4

99. Takumi, T., E. H. Yang, V. Mathew, C. S. Rihal, R. Gulati, L. O. Lerman, and A. Lerman. Coronary endothelial dysfunction is associated with a reduction in coronary artery compliance and an increase in wall shear stress. *Heart* , 2010.doi:10.1136/hrt.2009.187898

100. Talukder, M. A. H., W. M. Johnson, S. Varadharaj, J. Lian, P. N. Kearns, M. A. El-Mahdy, X. Liu, and J. L. Zweier. Chronic cigarette smoking causes hypertension, increased oxidative stress, impaired NO bioavailability, endothelial dysfunction, and cardiac remodeling in mice. *Am. J. Physiol. - Hear. Circ. Physiol.* , 2011.doi:10.1152/ajpheart.00868.2010

101. Tao, J., Y. F. Jin, Z. Yang, L. C. Wang, X. R. Gao, N. Lui, and H. Ma. Reduced arterial elasticity is associated with endothelial dysfunction in persons of advancing age: Comparative study of noninvasive pulse wave analysis and laser Doppler blood flow measurement. *Am. J. Hypertens.* , 2004.doi:10.1016/j.amjhyper.2004.03.678

102. Tedesco, M. A., F. Natale, G. Di Salvo, S. Caputo, M. Capasso, and R. Calabró. Effects of coexisting hypertension and type II diabetes mellitus on arterial stiffness. *J. Hum. Hypertens.* , 2004.doi:10.1038/sj.jhh.1001690

103. Tejero, J., and D. Stuehr. Tetrahydrobiopterin in nitric oxide synthase. *IUBMB Life* 65:358–365, 2013.

104. Tesauro, M., A. Mauriello, V. Rovella, M. Annicchiarico-Petruzzelli, C. Cardillo, G. Melino, and N. Di Daniele. Arterial ageing: from endothelial dysfunction to vascular calcification. , 2017.doi:10.1111/joim.12605

105. Thacher, T. N., P. Silacci, N. Stergiopulos, and R. F. Da Silva. Autonomous effects of shear stress and cyclic circumferential stretch regarding endothelial dysfunction and oxidative stress: An ex vivo arterial model. *J. Vasc. Res.* , 2010.doi:10.1159/000265567

106. Tong, J., F. Yang, X. Li, X. Xu, and G. X. Wang. Mechanical Characterization and Material Modeling of Diabetic Aortas in a Rabbit Model. *Ann. Biomed. Eng.* , 2018.doi:10.1007/s10439-017-1955-9

107. Torres, W. M., S. C. Barlow, A. Moore, L. A. Freeburg, A. Hoenes, H. Doviak, M. R. Zile, T. Shazly, and F. G. Spinale. Changes in Myocardial Microstructure and Mechanics With Progressive Left Ventricular Pressure Overload. *JACC Basic to Transl. Sci.* , 2020.doi:10.1016/j.jacbts.2020.02.007

108. Tounian, P., Y. Aggoun, B. Dubern, V. Varille, B. Guy-Grand, D. Sidi, J. P. Girardet, and D. Bonnet. Presence of increased stiffness of the common carotid artery and endothelial dysfunction in severely obese children: A prospective study. *Lancet* , 2001.doi:10.1016/S0140-6736(01)06525-4

109. Tudoran, M., and C. Tudoran. Particularities of endothelial dysfunction in hypothyroid patients. *Kardiol. Pol.* , 2014.doi:10.5603/KP.a2014.0241

110. Ungvari, Z., S. Tarantini, T. Kiss, J. D. Wren, C. B. Giles, C. T. Griffin, W. L. Murfee, P. Pacher, and A. Csiszar. Endothelial dysfunction and angiogenesis impairment in the ageing vasculature. , 2018.doi:10.1038/s41569-018-0030-z

111. Valentín, A., L. Cardamone, S. Baek, and J. D. Humphrey. Complementary vasoactivity and matrix remodelling in arterial adaptations to altered flow and pressure. *J. R. Soc. Interface* , 2009.doi:10.1098/rsif.2008.0254

112. Valentín, A., and J. D. Humphrey. Parameter sensitivity study of a constrained mixture model of arterial growth and remodeling. *J. Biomech. Eng.* , 2009.doi:10.1115/1.3192144

113. Valentín, A., J. D. Humphrey, and G. A. Holzapfel. A multi-layered computational model of coupled elastin degradation, vasoactive dysfunction, and collagenous stiffening in aortic aging. *Ann. Biomed. Eng.* , 2011.doi:10.1007/s10439-011-0287-4

114. Valentín, A., J. D. Humphrey, and G. A. Holzapfel. A finite element-based constrained mixture implementation for arterial growth, remodeling, and adaptation: Theory and numerical verification. *Int. j. numer. method. biomed. eng.* , 2013.doi:10.1002/cnm.2555

115. Vanhoutte, P. M., H. Shimokawa, E. H. C. Tang, and M. Feletou. Endothelial dysfunction and vascular disease. , 2009.doi:10.1111/j.1748-1716.2009.01964.x

116. Wagenseil, J. E., and R. P. Mecham. Vascular extracellular matrix and arterial mechanics. , 2009.doi:10.1152/physrev.00041.2008

117. Wagenseil, J. E., and R. P. Mecham. Elastin in large artery stiffness and hypertension. *J. Cardiovasc. Transl. Res.* , 2012.doi:10.1007/s12265-012-9349-8

118. Wan, W., J. B. Dixon, and R. L. Gleason. Constitutive modeling of mouse carotid arteries using experimentally measured microstructural parameters. *Biophys. J.* , 2012.doi:10.1016/j.bpj.2012.04.035

119. Wan, W., L. Hansen, and R. L. Gleason. A 3-D constrained mixture model for mechanically mediated vascular growth and remodeling. *Biomech. Model. Mechanobiol.* , 2010.doi:10.1007/s10237-009-0184-z

120. Watson, S. R., P. Liu, E. A. Peña, M. A. Sutton, J. F. Eberth, and S. M. Lessner. Comparison of Aortic Collagen Fiber Angle Distribution in Mouse Models of Atherosclerosis Using Second-Harmonic Generation (SHG) Microscopy. *Microsc. Microanal.* 22:55–62, 2016.

121. Wilkinson, I. B., H. Maccallum, D. F. Rooijmans, G. D. Murray, J. R. Cockcroft, J. A. McKnicht, D. J. Webb, and L. Wilkinson. Increased augmentation index and systolic stress in type 1 diabetis mellitus. *QJM - Mon. J. Assoc. Physicians* , 2000.doi:10.1093/qjmed/93.7.441

122. Wilstein, Z., D. M. Alligood, V. L. McLure, and A. C. Miller. Mathematical model of hypertension-induced arterial remodeling: A chemo-mechanical approach. *Math. Biosci.* , 2018.doi:10.1016/j.mbs.2018.05.002

123. Woo, K. S., P. Chook, C. W. Yu, R. Y. T. Sung, M. Qiao, S. S. F. Leung, C. W. K. Lam, C. Metreweli, and D. S. Celermajer. Overweight in children is associated with arterial endothelial dysfunction and intima-media thickening. *Int. J. Obes.* , 2004.doi:10.1038/sj.ijo.0802539

124. Wu, G., and C. J. Meininger. Nitric oxide and vascular insulin resistance. , 2009.doi:10.1002/biof.3

125. Wu, J., and S. C. Shadden. Coupled Simulation of Hemodynamics and Vascular Growth and Remodeling in a Subject-Specific Geometry. *Ann. Biomed. Eng.* , 2015.doi:10.1007/s10439-015-1287-6

126. Wu, J., and S. C. Shadden. Stability analysis of a continuum-based constrained mixture model for vascular growth and remodeling. *Biomech. Model. Mechanobiol.* , 2016.doi:10.1007/s10237-016-0790-5

127. Yamazaki, Y., and Y. Kamiyama. Mathematical model of wall shear stress-dependent vasomotor response based on physiological mechanisms. *Comput. Biol. Med.* , 2014.doi:10.1016/j.compbiomed.2013.11.018

128. Yang, S., Y. Qi, Z. Jiang, and X. Gong. Characterizing the mechanical variations of human femoropopliteal artery during aging process. *MCB Mol. Cell. Biomech.* 16:13–26, 2019.

129. Yang, Y. M., A. Huang, G. Kaley, and D. Sun. eNOS uncoupling and endothelial dysfunction in aged vessels. *Am. J. Physiol. - Hear. Circ. Physiol.* , 2009.doi:10.1152/ajpheart.00230.2009

130. Yuksel, M., A. Yildiz, M. Oylumlu, F. M. Turkcu, M. Z. Bilik, A. Ekinci, B. Elbey, E. Tekbas, and S. Alan. Novel markers of endothelial dysfunction and inflammation in Behçet's disease patients with ocular involvement: epicardial fat thickness, carotid intima media thickness, serum ADMA level, and neutrophil-to-lymphocyte ratio. *Clin. Rheumatol.* , 2016.doi:10.1007/s10067-015-2907-0

131. Zhou, B., A. Rachev, and T. Shazly. The biaxial active mechanical properties of the porcine primary renal artery. *J. Mech. Behav. Biomed. Mater.* 48:28–37, 2015.

132. Zulliger, M. A., A. Rachev, and N. Stergiopulos. A constitutive formulation of arterial mechanics including vascular smooth muscle tone. *Am. J. Physiol. - Hear. Circ. Physiol.* , 2004.doi:10.1152/ajpheart.00094.2004

Appendix A

Kinematic Definitions

Before the constitutive stress-strain relationships can be created, kinematic definitions must be set to the material in question. During model development, different choices must be made regarding the kinematic definitions. On the scale of the body for the entire vessel, most models use a first-order deformation gradient tensor to define the change in geometry from which the Cauchy-Green strain can be computed [22,113]. When the body is deformed, a stretch ratio is often used to compare the deformed to the undeformed geometries [83,84,125]. In an experimental setting, this deformation, is often calculated using an inflation-extension test to simulate the *in-vivo* deformation of the elastic artery [122]. Some models then couple this with a defined opening angle from an artery cut into a sector, [113]. This method allows for the computation of the residual stress within the artery due to the interactions between collagen and elastin [113,114].

In the kinematic definitions for microstructurally based models, the kinematics for each constituent must be defined. Because of its typically membranous nature in the elastic arteries, elastin is normally defined as an isotropic material with no directionality and assumes a factor of the deformation of the entire body [86,122]. Kinematically, smooth muscle is defined in a similar fashion but with a slight directionality [132]. Smooth muscle is normally oriented in a way that

almost circumferentially wraps around the artery, causing it to have transversely orthotropic behavior with a tendency toward the circumferential direction [54,122]. However, recent evidence suggests that smooth muscle orientation is more complex, so future models might account for vascular SMC's to have more of a Gaussian distribution with helical domains [98].

Collagen, on the other hand, is commonly defined as a distribution of fibers, with multiple fiber families each with a directional orientation [83,113,119,125]. Previous studies group the collagen fibers into two families based on angle relative to the axial/longitudinal direction, in which the fiber length and angle relative to the axial direction are defined in both the stress-free and loaded configurations (**Figure 3.1**) [119]. However, recent works use more fiber families to account for the increased complexity of the collagen fiber network [83,126]. This expansion to four collagen fiber families allows for the inclusion of fibers that are oriented in the radial direction and those that are in compression at any given stress state [83].

Another use of the four-fiber family model is to assume the directionality of two main collagen fiber families to be in alignment with the principal stresses and assuming the other families to be oriented in the circumferential and axial directions, respectively [54]. However, it is possible that using a lower number of fiber families maintains the purpose of simplifying the problem and assuming the contributions from those other two families to be negligible. In future studies, the multi-fiber family model may be abandoned for a more complex, Gaussian, beta, or von Mises mixture distribution to account for the true nature of the structure of collagen within the arterial extracellular matrix [50,118]. As more evidence behind the

true distribution of collagen fibers within the vascular extracellular matrix is compiled, the need for more biomechanical models that utilize this description becomes evident [65,118].

Appendix B

Constitutive Equations

After the kinematics of the vessel in question are defined, constitutive equations can then be formulated to relate deformations in the healthy blood vessel geometry to the stress and strain of the tissue. As with defining the kinematics, the strain energy functions for each constituent must be defined before attempting to define the behavior for the entire vessel. In most models, elastin is assumed to be an isotropic, homogeneous material that demonstrates simple neo-Hookean behavior based on the first tensor invariant [51,83,113,119]. This assumption is reasonable due to the membranous nature of most of the elastin found in the elastic arteries and mostly simple elastic behavior of the collagen fibers [65,86].

In the passive state completely without contractile activity, smooth muscle is commonly defined as a transversely isotropic material with preference toward the circumferential direction [86,119]. Mathematically, this transverse isotropy is modeled within the strain energy function through the normal circumferential stress displaying dependency on direct material properties while stress along the other directions displays the previously defined simple elastic behavior [50,51,126]. However, other studies have considered the smooth muscle's elastic contributions in the radial and axial directions to be negligible compared to that of the other constituents, further simplifying this strain energy function [8].

While constitutive equations for the other constituents are simpler due to their lack of material complexity, definitions of the collagen fiber matrix must account for its directional distribution in addition to the mechanical properties of the individual fibers. Individually, collagen fibers display orthotropic behavior with different mechanical properties in each orthogonal direction [83,84,119]. Some models accomplish this by multiplying the properties of the individual fiber families by the direction vector for that family along the axial-circumferential plane [119,125]. Others display this directionality using an orientation angle along the axial-circumferential plane while applying vector directionality to families not oriented along the major load-bearing plane [83,84]. Still others expand upon this formulation by describing collagen using a distribution with a majority of fibers oriented along a principal direction [65]. These models can be further expanded upon by accounting for the separate mechanical properties that arise from density-dependent collagen cross-linking [89].

While previous models have assumed the arterial extracellular matrix to act akin to a fiber-reinforced mixture, recent models add additional complexity to the collagen contribution by accounting for the recruitment of individual collagen fibers [65,83]. Using multiphoton microscopic imaging techniques, researchers in the field have shown that collagen not only has a directionality, but also a level of tortuosity (ratio of total length to straight length) [29]. As such, recent models account for this fiber tortuosity by assuming that a collagen fiber only becomes loadbearing when it becomes completely uncoiled (i.e. tortuosity=1) [83]. In comparison to the simpler method which does not account for undulation, this method adds detail while also

requiring a deeper understanding of the collagen matrix of the desired arterial tissue. As such, more in-depth experimental analyses of the tissue in question are required to effectively utilize this added level of complexity.

To account for the combination of constituents in the total stress equations, most microstructurally based methods utilize a constrained mixture model. In this model, a strain energy function for the entire structure is created by multiplying the individual strain energy functions by the mass fractions of the corresponding load-bearing constituents [8,83]. For collagen, this includes a summation of the strain energy contributions of each fiber family [8,83]. Once the strain energy function is defined, many theoretical frameworks compute the stress equation through a modification of the strain energy derivative with respect to the right Cauchy-Green strain tensor, as is clearly presented in Bellini, et al. [8]. One major assumption for most biological tissue that is accounted for in the formulation of the stress equation is that of incompressibility [8,83,84,86].

Additionally, smooth muscle cell activity must be considered in live arterial tissue. While some models account for this through an addition of an active stress tensor to denote the difference between the active and passive states, others account for the contribution of smooth muscle activity through the assumed circumferential directionality [8,119,125]. This additional directionality of smooth muscle cell activity provides for a more descriptive model of the active stress contribution. However, one might find it more difficult to translate this term to the experimental setting. Nonetheless, the active stress contribution of both models fails to account for the more complex mediation of vascular smooth muscle cell activity that occurs

in response to internal and external stimuli. To account for the true interaction of the vascular wall with the mechanical stimulus of blood flow, a fluid-structure-interaction model should be considered [16,39]. To include the true activity of smooth muscle cells *in-vivo*, one might incorporate chemo-mechanical components that account for the presence of internal and external signaling molecules [53].

Appendix C

Growth and Remodeling

To effectively account for restructuring that occurs during vascular pathologies like endothelial dysfunction, growth and remodeling elements would likely need to be added to the established constitutive equations. During growth and remodeling (G&R), the relative amounts of the constituents, notably collagen, changes to adapt to a long-term change in the loads experienced by the vessel wall [1]. The altered composition manifests itself in a change in the vessel geometry, as shown in **Figure 3.2** [51]. This change is often characterized by a remodeling stretch ratio resulting in two new mechanical states: an unloaded remodeled state and a loaded remodeled state [51,84].

Regarding the total amount of constituents, some models may assume that the total change in the amount of elastin in the arterial wall is almost negligible compared to gross deposition and restructuring of the collagen matrix [83]. However, if one is to accurately describe the structural changes that occur due to endothelial dysfunction, one must account for the slow degradation of elastin that is documented in many histological samples [65,104]. One method to account for this is through a simple first-order decay function, which provides utility in its simplicity and adequate accuracy [114,126]. Other models take a more complex approach, assuming the same growth and decay equations for all constituents and then

modifying their approaches to account for the increased complexity that accompanies the collagen matrix [119].

In some cases, complexity is even further derived through the addition of kinetic definitions to account for these constitutive changes, especially in terms of collagen. Some models start with the assumption of conservation of mass density and assume that the total change in mass is equal to the difference in mass production and mass removal [12,119]. In some cases, the new stress contribution by the generated collagen is then assumed to relieve some of the stress previously supplied by smooth muscle activity [8,119]. This is often incorporated in a stress-dependent mass production/degradation equation [12,89]. Other models take a simpler approach, employing a basal production and degradation rate of collagen independent of the active stress generation [51,125].

Concerning the orientation of the newly produced collagen, most models argue that this collagen is in a singular or bimodal Gaussian-type distribution with a mean orientation in the same direction as that of the consistent abnormal stress [65,83]. This assumption would make sense due to the attempt in remodeling to restore circumferential stress experienced by the arterial wall to that of the healthy state [113,119]. In turn, the change in the overall collagen distribution due to turnover within the collagen matrix is accounted for via the collagen survival fraction, which shows the exponential decay of the collagen originally found within the healthy tissue [113,126]. Other recent studies have further improved upon this through the relationship between collagen remodeling and hemodynamic stress generation, considering the shear and normal stress interaction that the arterial wall is directly

experiencing due to blood flow and pressure [125]. While a chemo-mechanical model is normally used to account for the nuanced cellular interactions, some studies have found a balance with looking at signal concentrations within the continuum[89].